ORNL/TM-2005/241

Neutron Resonance Parameters of ^{238}U and the Calculated Cross Sections from the Reich-Moore Analysis of Experimental Data in the Neutron Energy Range from 0 keV to 20 keV

November 2005

Prepared by
H. Derrien
L. C. Leal
N. M. Larson
A. Courcelle

Nuclear Science and Technology Division (94)

Neutron Resonance Parameters of ^{238}U and the Calculated Cross Sections from the Reich-Moore Analysis of Experimental Data in the Neutron Energy Range from 0 keV to 20 keV

H. Derrien
L. C. Leal
N. M. Larson
Oak Ridge National Laboratory,
P.O. Box 2008,
Oak Ridge, Tennessee 37831-6171, USA

A. Courcelle
Centre d' Etudes de Cadarache,
St. Paul-lez- Durance, 13108 FRANCE

November 2005

CONTENTS

iii

LIST OF FIGURES

LIST OF FIGURES (continued)

vi

LIST OF TABLES

ACRONYMS AND ABBREVIATIONS

ANL   Argonne National Laboratory
CLM   Crystal Lattice Model
FGM   Free Gas Model
GELINA   Geel Linear Accelerator
ICSBEP   International Criticality and Safety Benchmark Evaluation Project
JAERI   Japan Atomic Energy Research Institute
NEA   Nuclear Energy Agency
OECD   Organization for Economic Cooperation and Development
ORELA   Oak Ridge Electron Linear Accelerator
ORNL   Oak Ridge National Laboratory
PIE   postirradiation examination
PWR   pressurized water reactors
SRI   shielded resonance integral
TOF   Time-of-flight
URR   unresolved resonance region
WPEC   Working Party on International Nuclear Data Evaluation Cooperation

x

ACKNOWLEDGMENTS

ABSTRACT

The neutron resonance parameters of ^{238}U were obtained from a SAMMY analysis of high-resolution neutron transmission measurements and high-resolution capture cross section measurements performed at the Oak Ridge Electron Linear Accelerator (ORELA) in the years 1970–1990, and from more recent transmission and capture cross section measurements performed at the Geel Linear Accelerator (GELINA). Compared with previous evaluations, the energy range for this resonance analysis was extended from 10 to 20 keV, taking advantage of the high resolution of the most recent ORELA transmission measurements. The experimental database and the method of analysis are described in this report. The neutron transmissions and the capture cross sections calculated with the resonance parameters are compared with the experimental data. A description is given of the statistical properties of the resonance parameters and of the recommended values of the average parameters. The new evaluation results in a slight decrease of the effective capture resonance integral and improves the prediction of integral thermal benchmarks by 70 pcm to 200 pcm.

1. INTRODUCTION

There have long been inconsistencies both in the neutron resonance parameters and in the measured capture cross sections of ^{238}U. In order to resolve the discrepancies, a task force was organized by the Nuclear Energy Agency (NEA) of the Organization for Economic Cooperation and Development (OECD) in 1982. The task force produced a set of resonance parameters in the energy range thermal to 10 keV; results were published by M. G. Sowerby and M. Moxon in 1994.[1] These resonance parameters were adopted in the most important nuclear data libraries. More recently,[2] analysis of various thermal reactor benchmarks showed that the values of k_{eff} were still underestimated; this could correspond to an overestimation of the ^{238}U capture cross section.

Within the Working Party on International Nuclear Data Evaluation Cooperation (WPEC) of the NEA, a subgroup was created in 2001 to address this reactivity underprediction problem. One immediate goal of this group was to include data not used in the Sowerby and Moxon analysis. The high-resolution neutron transmissions measured in 1988 at the Oak Ridge Electron Linear Accelerator (ORELA) by J. A. Harvey *et al.*[3] have not been taken into account, and the high-resolution capture measurements of Macklin *et al.*,[4] also performed at ORELA in 1988, had not been completely analyzed.

The aim of the present report is to present the results of a SAMMY[5] analysis of all the ORELA neutron transmission and capture cross section data. Greater accuracy of the capture cross section was expected and obtained from this analysis, and the resolved-resonance range was extended to the neutron energy of 20 keV. Data from the neutron transmission measurements performed recently at the Geel Electron Linear Accelerator (GELINA) with metallic and oxide samples at two temperatures, by Meister *et al.*,[6] were also analyzed, in order to check the accuracy of different models used for the Doppler broadening of the resonances. The work was performed within the framework of the Nuclear Criticality Safety Program at Oak Ridge National Laboratory (ORNL), and as an international cooperative effort within WPEC/NEA/ OECD.

2. THE EXPERIMENTAL DATABASE

The experimental database used in the SAMMY analysis is summarized in Table 1.

Two important series of neutron transmission measurements were performed by Olsen *et al*. at ORELA. The results of the first series of measurements were published in 1977.[7] The measurements were performed at a 41.7-m neutron flight path in the neutron energy range above 0.52 eV; the transmissions were measured at room temperature for seven metallic samples with thicknesses ranging from 0.0036 to 3.62 cm, with a nominal resolution of about 0.1 ns/m at high energy. This first series of measurements allowed accurate determination of the resonance parameters in the low-energy range. In the second series (published between 1979 and 1986),[8–11] the measurements were performed at a 155-m flight path in the neutron energy range up to 100 keV; transmissions were measured at room temperature for four metallic samples with thicknesses ranging from 0.076 to 3.62 cm, with a nominal resolution of about 0.025 ns/m in the high energy range of the data; the resolution allowed the data to be analyzed up to 10 keV neutron energy.

The experimental transmission data of Harvey *et al.* were published in 1988.[3] These measurements were performed at a 201.6-m flight path in the neutron energy range 1 to 100 keV; transmissions were measured at room temperature for sample thicknesses of 0.1748, 0.0396, and 0.01235 at/barn with a nominal resolution of about 0.01 ns/m in the neutron energy range above 5 keV; the analysis of these data allowed the resolved energy range to be extended up to 20 keV.

The most recent transmission measurements were published by Meister *et al*.[6] in 1997. These measurements were performed at GELINA at a 26.5-m flight path with metallic and oxide samples with thickness of 20 mg/cm^2 and 40 mg/cm^2 of uranium, at temperatures of 23.7 and 293.7 K, for the first *s*-wave resonances (6.67, 20.9, and 36.7 eV). The goal of the experiments was to check the accuracy of the models used to calculate the Doppler broadening of the resonances and their effects on the determination of the resonance parameters.

Two sets of experimental capture cross sections were used in the present analysis: the 1973 data of de Saussure *et al*.[12] and the 1991 data of Macklin *et al*.[4] The capture cross sections of de Saussure *et al.* were measured at ORELA for incident neutron energies between 5 eV and 100 keV at a 40-m flight path with samples of thicknesses 0.0028 and 0.0004 at/b; the cross section was normalized by the saturated-resonance technique with an accuracy varying from 5% at 1 keV to 10% at 100 keV. The capture cross sections of Macklin *et al.* were measured for incident neutron energies between 1 keV and 100 keV at the ORELA 150-m flight path, with a nominal resolution of about 0.03 ns/m comparable to Harvey transmission resolution, with sample thicknesses of 0.0031 and 0.0124 at/b. The cross sections were normalized on the area of very small resonances with an accuracy of 6 to 8%. Due to the relatively large sample thicknesses, the experimental cross sections (effective capture cross sections) have to be corrected for self-shielding and multiple scattering effects. The corrections were performed by de Saussure for cross sections averaged over large energy ranges; they were not performed by Macklin. In the present

work, the self-shielding and multiple-scattering effects were directly calculated by SAMMY for each experimental data point. Examples of the importance of the corrections are shown in Figs. 1 and 2.

Table 1. The experimental database used in the SAMMY analysis

Energy range of analysis	Reference	Measurement type	Sample thickness	Flight path length
0.0253 eV	Poenitz et al.[13] ANL (1981)	Activation		
Thermal range	Corvi et al.[14] GELINA (1997)	Capture TOF	U and UO_2 0.001 at/b	8.7 m
5 eV to 20 keV	Difilippo et al.[15] ORELA (1980)	Fission TOF		40.0 m
6 eV to 38 keV	Meister et al.[6] GELINA (1997)	Transmission TOF	U and UO_2 0.000046 at/b 0.00010 at/b	26.5 m
6 eV to 10 keV	de Saussure et al.[12] ORELA (1973)	Capture TOF	2 samples 0.00283 at/b 0.00040 at/b	40.0 m
0.5 eV to 1 keV	Olsen et al.[7] ORELA (1977)	Transmission TOF	7 samples 0.0002 to 0.175 at/b	42.0 m
0.3 keV to 10 keV	Olsen et al.[8] ORELA (1979)	Transmission TOF	4 samples 0.0038 to 0.175 at/b	150.0 m
0.25 keV to 20 keV	Macklin et al.[4] ORELA (1988)	Capture TOF	2 samples 0.0031 at/b 0.0124 at/b	150.0 m
1 keV to 20 keV	Harvey et al.[3] ORELA (1988)	Transmission TOF	3 samples 0.0124 to 0.175 at/b	200.0 m
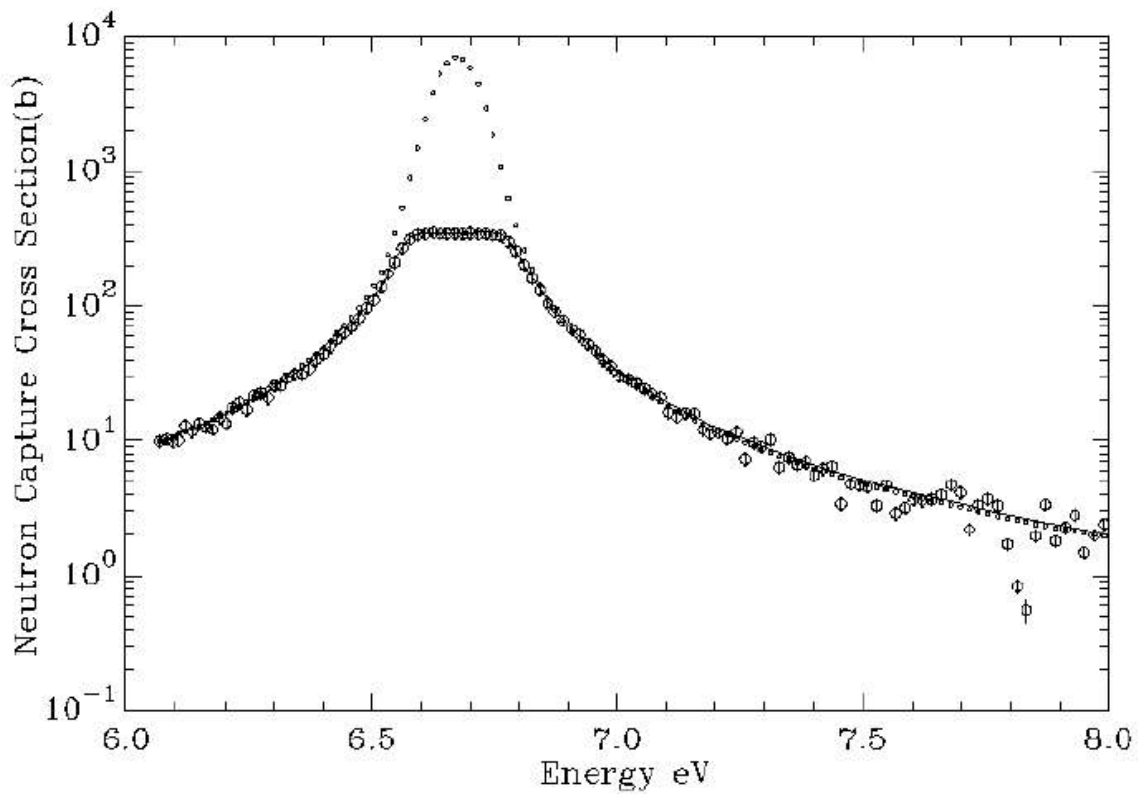
Fig. 1. The neutron capture cross section of ^{238}U near the 6.67-eV resonance. The large circles represent the de Saussure *et al*. experimental data points. The solid line represents the Doppler- and resolution-broadened capture cross section calculated from the resonance parameters, including self-shielding and multiple-scattering effects. The small circles represent the cross section calculated without self-shielding and multiple scattering effects.
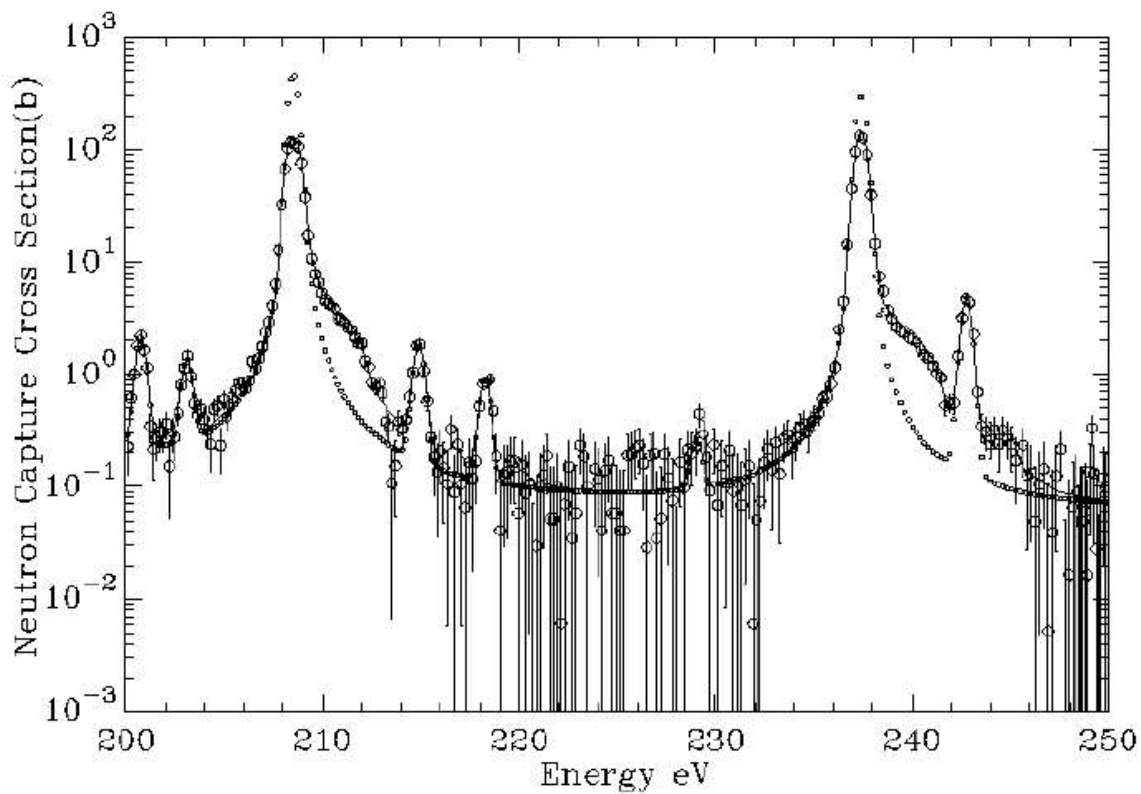
Fig. 2. The neutron capture cross section of ^{238}U in the energy range 200 to 250 eV. The large circles represent the de Saussure *et al*. experimental data points. The solid line represents the Doppler- and resolution-broadened capture cross section calculated from the resonance parameters, including self-shielding and multiple-scattering effects. The small circles represent the cross section calculated without self-shielding and multiple scattering effects.

In the thermal energy range, the Poenitz et al.[13] capture measurement at 0.0253 eV was used to normalize the capture cross section calculated with the resonance parameters. The capture cross sections measured at GELINA by Corvi et al.[14] in the energy range 0.001 to 0.08 eV were used to check the shape of the cross section in the thermal energy range.

In neutron time-of-flight (TOF) measurements, the accuracy in the determination of the neutron energy depends mainly on the accuracy of the neutron flight path length and on the accuracy of the neutron flight time. In the present analysis, the TOF measurements were precisely aligned on a common energy scale by using the relation $E' = aE + bE^{3/2}$, with a depending on the accuracy of the flight path length and b on the accuracy of the neutron flight time. The energy scale of the high-resolution transmission measurements of Harvey et al. was chosen as standard since these measurements were performed on the longest flight path, whose length had been determined with great accuracy at ORELA. For each measurement, the coefficients a and b were obtained by comparing the energies of several isolated resonances with the corresponding energies measured in Harvey data. This adopted energy scale agrees with the standard energy scale recommended by Mughabghab[16] for ^{238}U from the work of James et al.[17]

3. THE METHOD OF ANALYSIS

The analysis code SAMMY uses the multilevel, multichannel Reich-Moore[18] formalism for calculation of the reaction cross sections, and Bayes' method for fitting of experimental cross sections. Uncorrelated sets of experimental data are sequentially analyzed. The covariance file (which contains both the resonance parameters and the associated covariance matrix for these parameters) obtained from analysis of a set of experimental data is used as input for analysis of the next set of experimental data. The R-matrix nuclear reaction theory is a good description of the experimental data, provided that experimental effects are properly taken into account. These effects include Doppler- and resolution-broadening, self-shielding and multiple scattering corrections in the sample, and normalization and/or background corrections.

When analyzing a single set of data which contains very small experimental errors, in principle a unique set of resonance parameters can be obtained for the exact representation of all the data. However, in practical situations, the experimental data include small or large measurement errors, known or unknown, which could cause a set of several uncorrelated results to be inconsistent. In order to perform a consistent analysis of all experimental data, one should take into account in the SAMMY calculations the systematic measurement uncertainties (primarily normalization and background correction uncertainties), for which partial information could be found in the publications by the authors of the experiments. The knowledge of the experimental correction parameters is particularly important for determination of the long-range correlations in the final parameter covariance matrix.

Practical considerations do not always permit the optimal procedures. In the present work, the size of the experimental database was very large; the total number of data points of the experimental database was about 500,000. A single correlated SAMMY run, covering the entire energy range with all the selected experimental data, was not possible. The SAMMY analyses were performed in partial energy ranges of 1 keV for the energy region from 1 to 20 keV. At energies below 200 eV, the large s-wave resonances were analyzed resonance by resonance. Consequently, only partial correlation matrices were obtained. Nevertheless the long-range correlations between resonance parameters were found to be small, and a reasonably accurate full correlation matrix could be obtained by assembling the partial matrices.

The correction parameters (normalization and background) are strongly correlated to the unknown contribution of the resonances external to the energy range analyzed (negative-energy resonances and resonances in the energy range above 20 keV), and to the effective scattering radius R′. In the most recent ORELA transmission measurements (by Harvey $et\ al.$), the normalization factors are known with an accuracy better than 1%, and the errors due to the background evaluation are very small.[19] Therefore, the scattering radius and the contribution of the external resonances could be determined from the Harvey transmission data with negligible background and normalization corrections. Preliminary SAMMY fits were performed on the transmission data of Harvey $et\ al.$ in order to obtain the best values for the scattering radius and for the parameters describing the

contribution of the external resonances. The value of 9.48 fm was obtained for R'. This value was held fixed for the remainder of the evaluation.

In the first analysis of his experimental data, Olsen[7,8] obtained the value of 9.45 ± 0.05 fm in the energy range below 800 eV and 9.48 ± 0.06 fm in the energy range 880 to 2230 eV. In the final analysis of the 155-m transmission data,[11] he obtained the values of 9.66, 9.71, and 9.64 fm in the energy ranges 1 to 4 keV, 4 to 7 keV, and 7 to 10 keV, respectively. Since R' is strongly correlated to the external resonance parameters, it is likely that the difference between his results and the present analysis are mainly due to a different evaluation of the contribution of the external resonances. Actually, Olsen calculates the contribution of the external levels with an equation obtained from a picket-fence model of resonances at negative energies and at energies above 10 keV. The parameters in this equation were not adjusted to produce a constant value of R' in the energy range 0 to 10 keV. The only adjustment of the external resonance parameters by Olsen[7] was performed for the analysis of the resonances at 6.67, 20.9, and 36.8 eV leading to R' values between 9.45 and 9.49 fm. The effective scattering radius is related to the nuclear radius r by $R' = r(1 - R^{\infty})$, R^{∞} being the parameter which represents the contribution of more distant levels. In SAMMY the nuclear radius is calculated by the relation $1.23A^{1/3} + 0.8$ fm, and for $R' = 9.48$ fm R^{∞} is -0.126.

Experimental resolution- and Doppler-broadening parameters are needed for an accurate description of the resonance shape. For the resolution parameters, the contributions of some components (such as the TOF channel width and the accelerator electron burst width) are straightforward. Others needed to be checked, particularly the contribution of the neutron moderator and of the neutron detector in the transmission measurements, both of which contribute to an asymmetric tail in the resolution function. In SAMMY the asymmetric tail is an exponential characterized by a "half-life" τ that may vary with the energy of the neutron. In the resonance analysis of the ^{239}Pu transmission data of Harvey et al.,[3] which were measured with the same experimental conditions as ^{238}U, it was found[20] that the parameter τ varied as $1/E^{1/2}$, with a value of 88 ± 9 ns at 100 eV neutron energy. Preliminary shape analysis of the Harvey ^{238}U transmission data in isolated resonances (or groups of resonances) in the energy range 10 to 20 keV gave for τ the value of 107 ± 10 ns at 100 eV. The importance of using a realistic asymmetric shape for the resolution function was stressed by Olsen et al.[8] The neutron widths, in the neutron energy range 1 to 5 keV, increased by a few percent when the data were fitted by an asymmetric resolution function instead of a Gaussian function. The same method of shape analysis of isolated resonances was also applied to the Olsen 1978 high-energy transmission data, leading to a value for τ of 220 ± 30 ns at 100 eV; this value is different from the one found for the Harvey transmission data due to a different neutron lithium-glass detector. For the Olsen 1977 low-energy data, a constant value of 30 ns was obtained from the shape analysis of isolated resonances.

In SAMMY, Doppler broadening of resonances can be calculated by the Lamb[21] Free Gas Model (FGM) or by the Crystal Lattice Model (CLM) taken from the code DOPUSH.[22] The FGM model was used in the energy range above 100 eV, with an effective temperature of 300 ± 5 K, since all the data above 100 eV were taken with samples at room temperature. Both FGM and CLM models were used for the analysis of the GELINA data, taken at 23 K and at room temperature, in

order to check the effect of the model on the neutron and capture widths of the low-energy s-wave resonances. (It is assumed that this effect is unimportant in the high-energy ranges, where the error on the resonance parameters is mainly due to the errors on the experimental resolution widths.)

4. RESULTS OF THE ANALYSIS: THE AVERAGE NEUTRON TRANSMISSIONS AND CROSS SECTIONS

Examples of SAMMY fits are shown in Figs. 3–12. In each figure, the experimental data are given and compared with the values calculated with the resonance parameters. In the energy range 1 to 20 keV, the final SAMMY fits of the neutron transmission data were performed without normalization or background corrections; for the thick and medium sample transmission data of Harvey *et al.*, shown in Table 2, the agreement between the experimental and calculated values is much better than 1% (0.10% on average for the thick sample and 0.60% on average for the medium sample). The Olsen thick-sample experimental data are on average 0.5% smaller than the calculated values in the energy range 1 to 10 keV.

Below 1 keV, the preliminary SAMMY fits of the Olsen data showed an overestimation of the experimental background, which was apparent in the black resonances. For the 0.174-at/b sample, the background correction was $0.0017 + 0.0025/E^{1/2}$, corresponding to about 0.7% and 1.0% of the average transmission at 6 eV and 1 keV, respectively. For the 0.052-at/b sample, the correction was about 0.002 at all energies, corresponding to 0.4% of the average transmission. The correction for the thin samples seemed to be negligible (less than 0.1% of the average transmission).
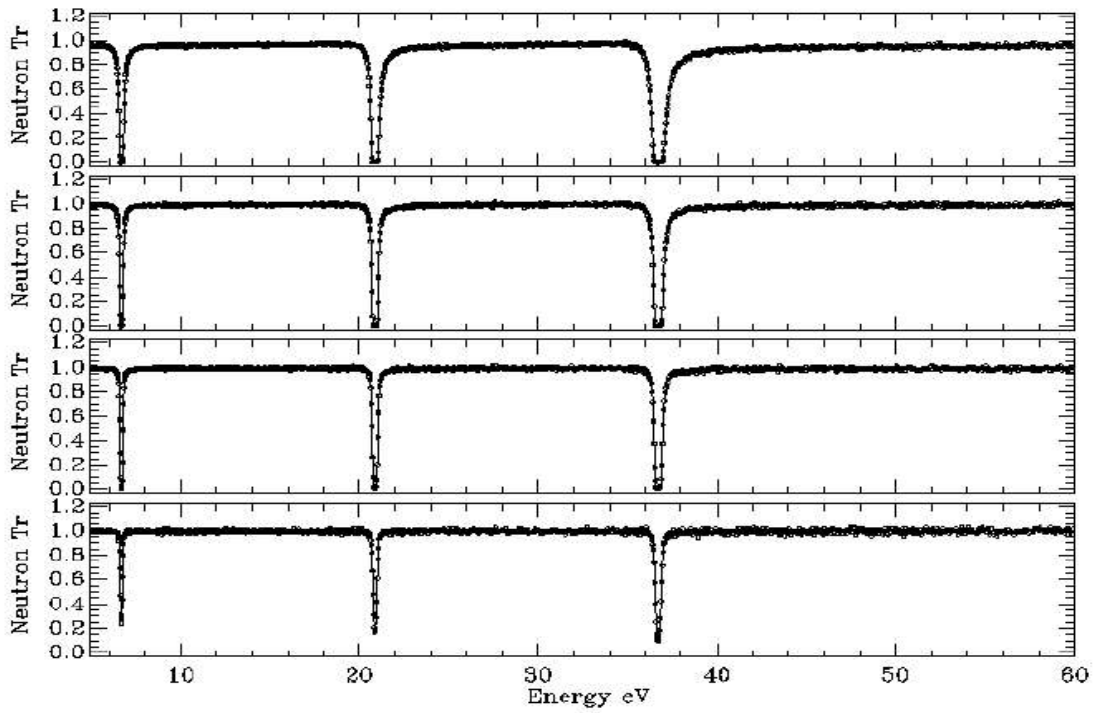
Fig. 3. The neutron transmission of [238]U in the neutron energy range 0.6 to 60 eV through sample thicknesses of 0.0762, 0.0254, 0.0127, and 0.0038 cm, respectively, from the upper curve to the lower curve. The circles represent the experimental data of Olsen *et al*. The solid lines are the results of the SAMMY fits.
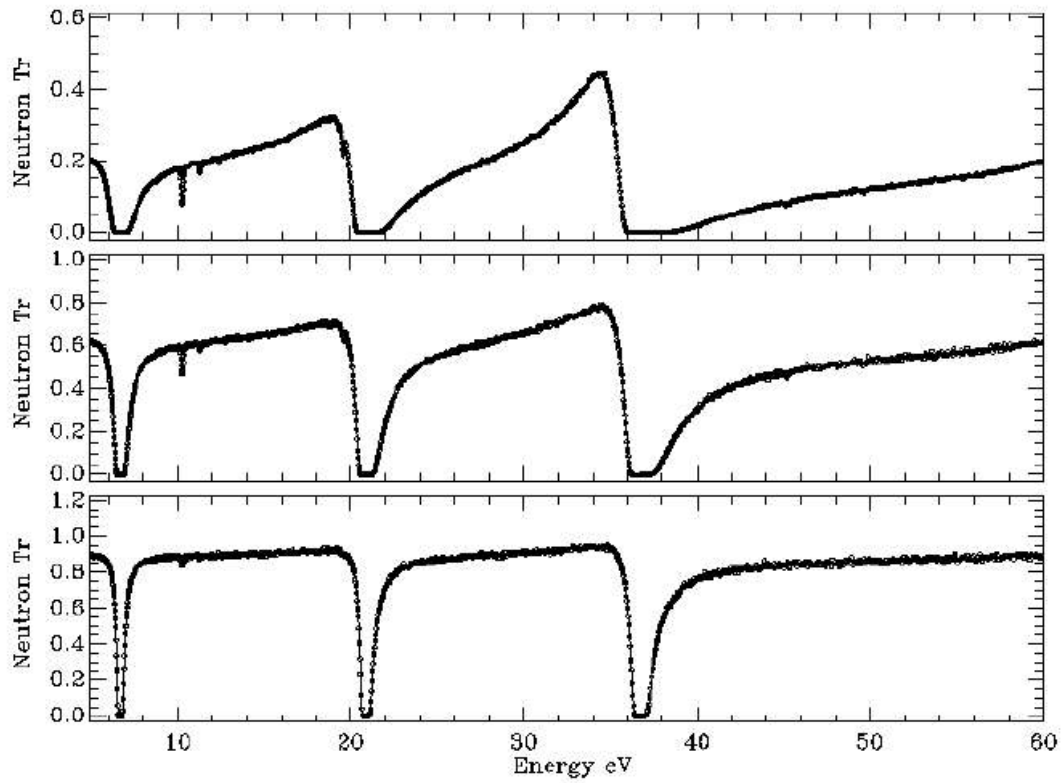
Fig. 4. **The neutron transmission of ^{238}U in the neutron energy range 0.6 to 60 eV through sample thicknesses of 3.62, 1.08, and 0.254 cm, respectively, from the upper curve to the lower curve.** The circles represent the experimental data of Olsen *et al*. The solid lines are the results of the SAMMY fits.
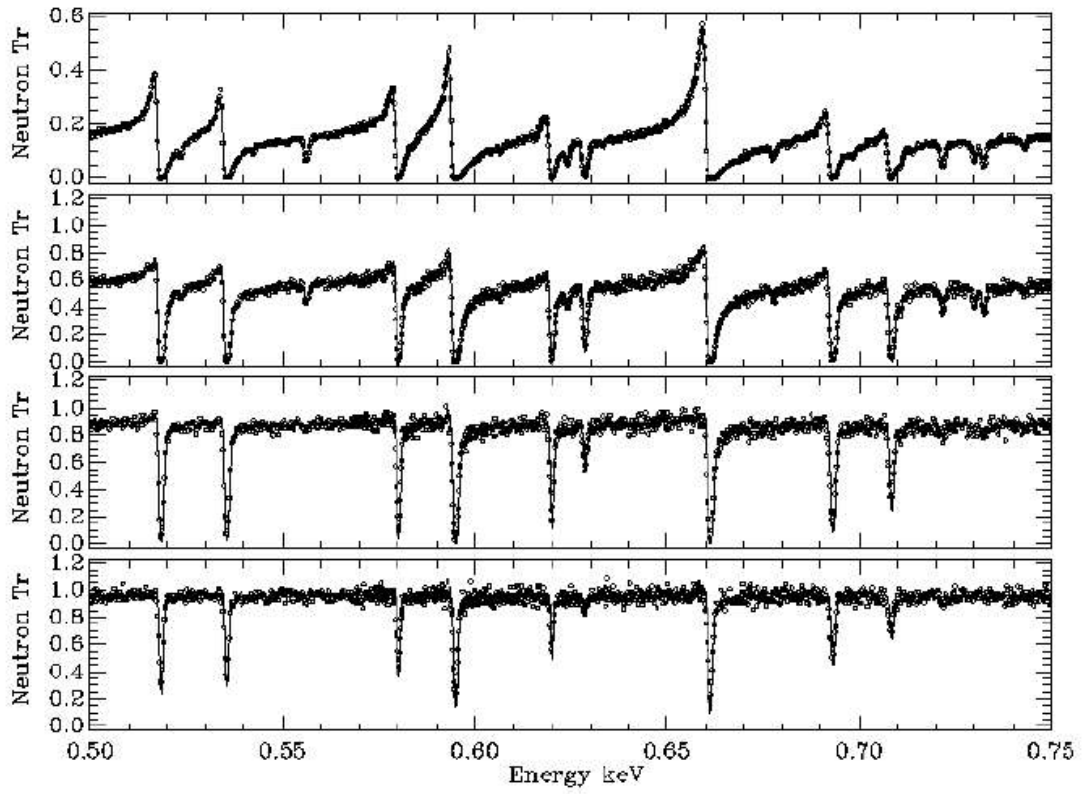
Fig. 5. The neutron transmission of [238]U in the neutron energy range 500 to 750 eV through sample thicknesses of 3.62, 1.08, 0.254, and 0.076 cm, respectively, from the upper curve to the lower curve. The circles represent the experimental data of Olsen *et al*. The solid lines are the results of the SAMMY fits.
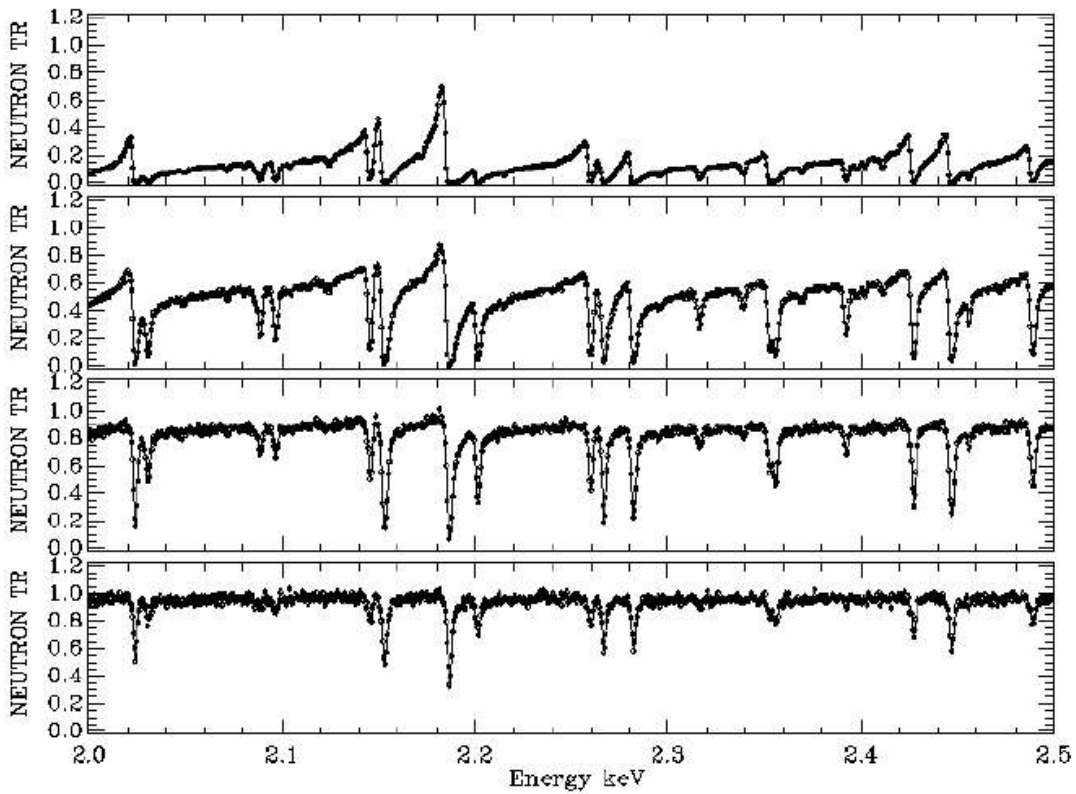
Fig. 6. The neutron transmission of ^{238}U in the neutron energy range 2.0 to 2.5 keV through sample thicknesses of 3.62, 1.08, 0.254, and 0.076 cm, respectively, from the upper curve to lower curve. The circles represent the experimental data of Olsen *et al*. The solid lines are the results of the SAMMY fits.

< 2>
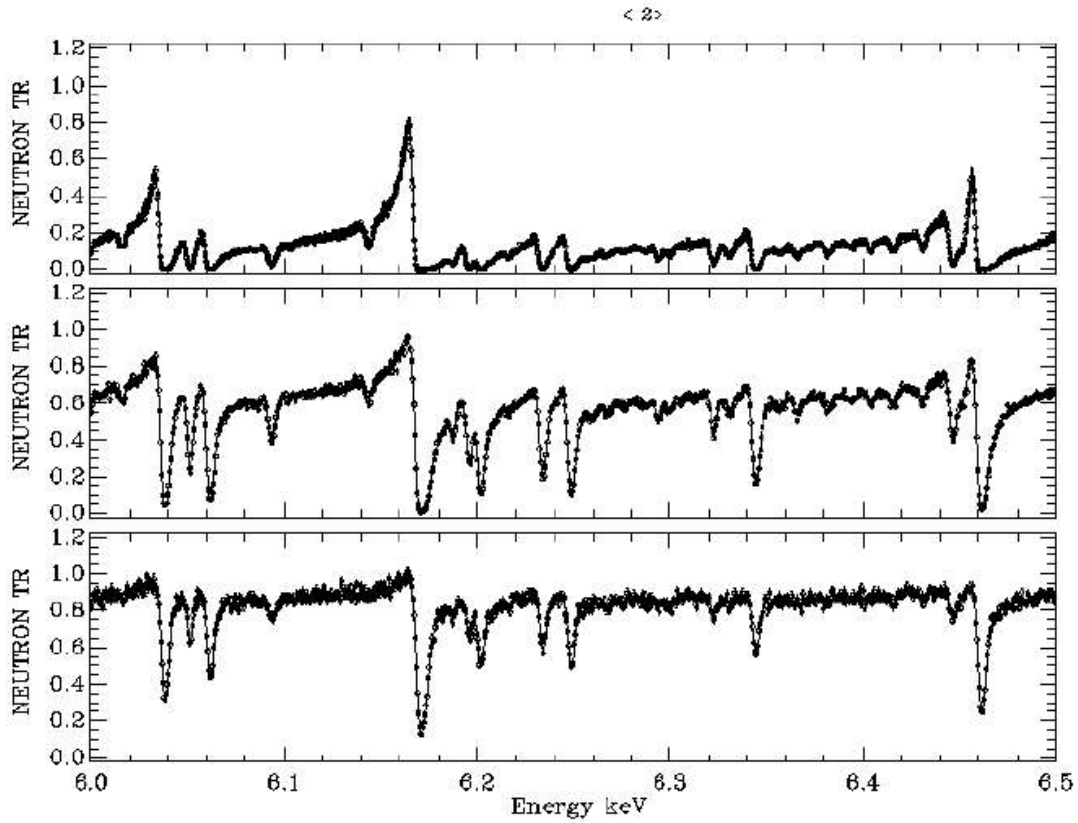
Fig. 7. The neutron transmission of ^{238}U in the neutron energy range 6.0 to 6.5 keV through sample thicknesses of 3.62, 0.250, and 0.083 cm, respectively, from the upper curve to the lower curve. The circles represent the experimental data of Harvey *et al*. The solid lines are the results of the SAMMY fits.

< 2>
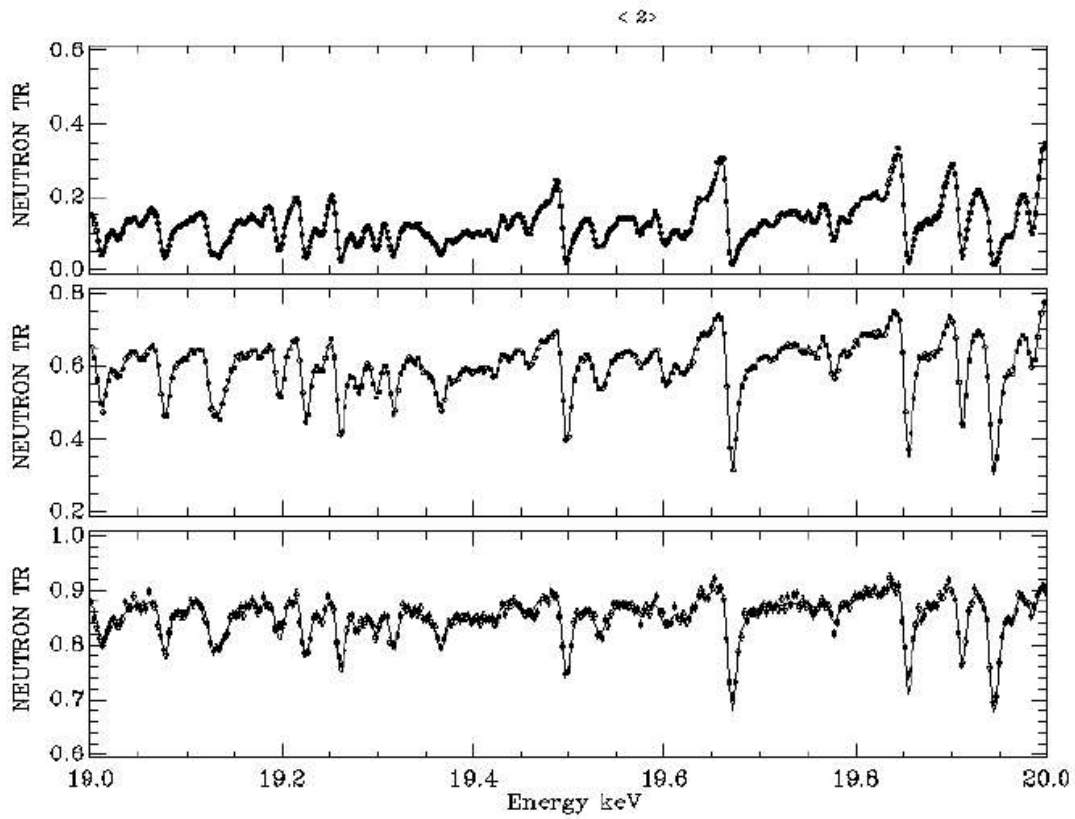
Fig. 8. The neutron transmission of ^{238}U in the neutron energy range 19.0 to 20.0 keV through sample thicknesses of 3.62, 0.250, and 0.083 cm, respectively, from the upper curve to the lower curve. The circles represent the experimental data of Harvey *et al*. The solid lines are the results of the SAMMY fits.

< 2>
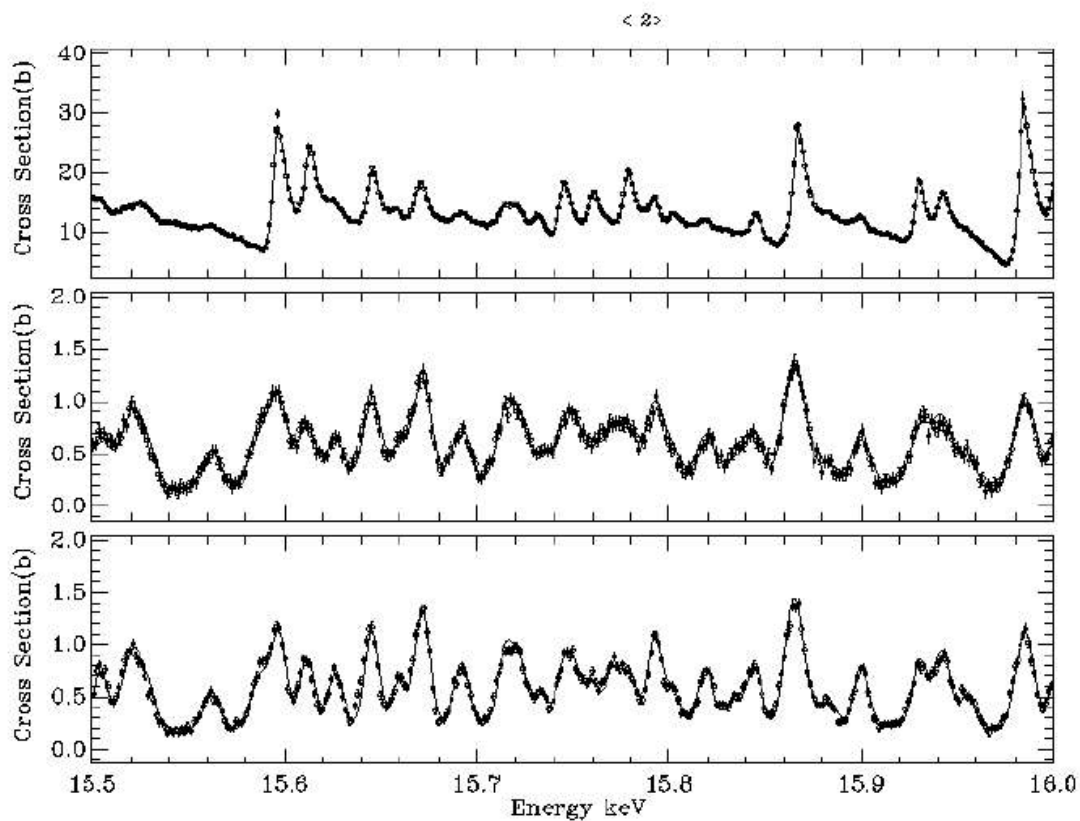
Fig. 9. The neutron effective total cross section and effective capture cross section of ^{238}U in the neutron energy range 15.5 to 16.0 keV. The circles represent the experimental data of Harvey *et al.* for the 3.62-cm sample (upper curve), and the experimental capture data of Macklin *et al.* for the 0.0031 and 0.0124 at/b samples (middle and lower curves, respectively). The solid lines are the results of the SAMMY fits.
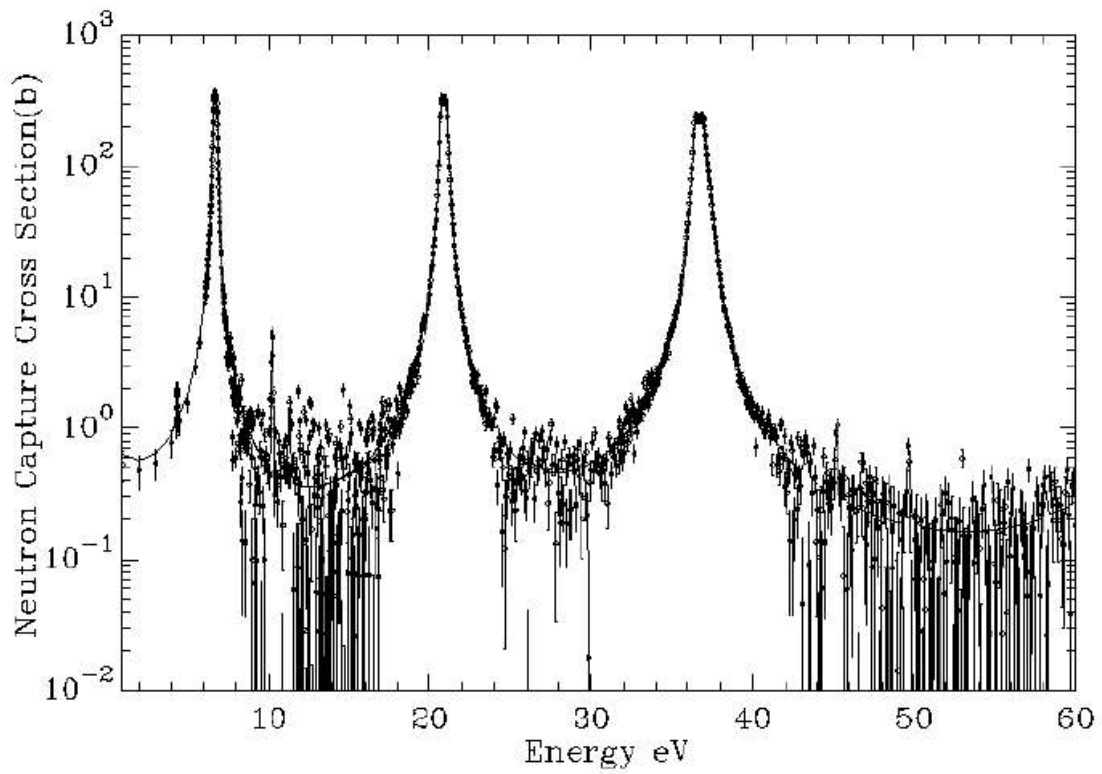
Fig. 10. The neutron capture cross section in the energy range 1 to 60 eV. The circles with the errors bars represent the experimental data of de Saussure *et al*. The solid line is the result of the SAMMY fit with the self-shielding and multiple- scattering effects.

21
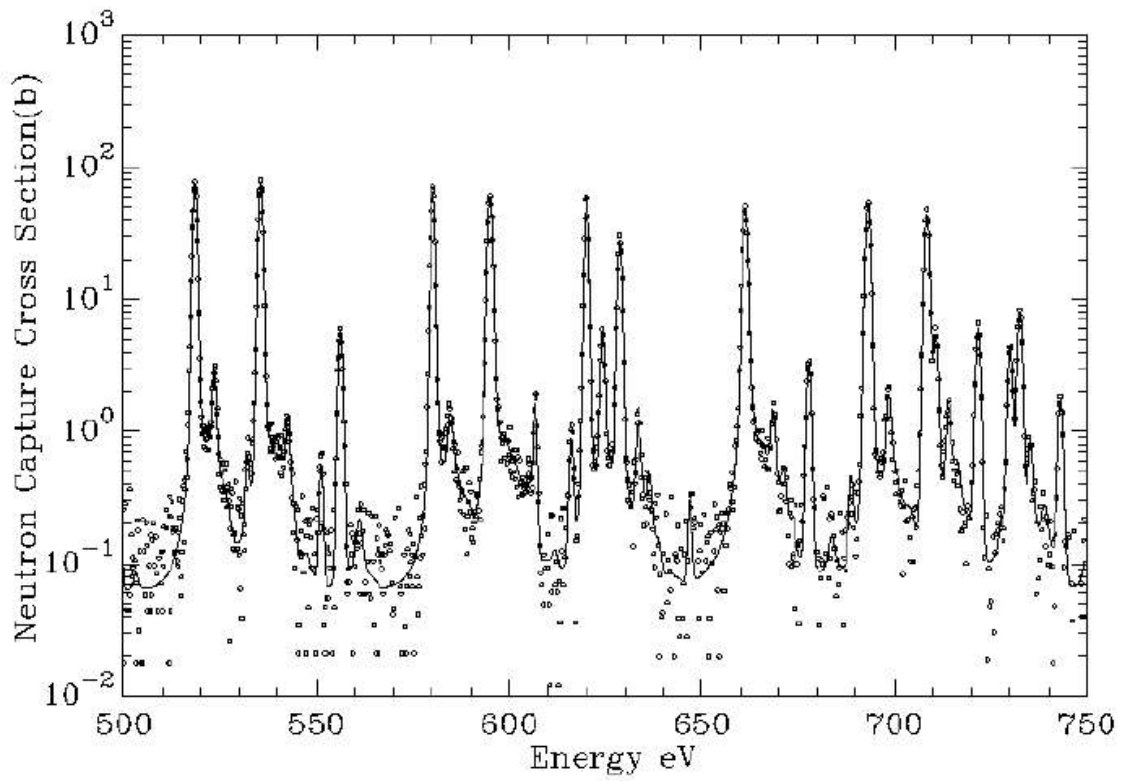
Fig. 11. The neutron effective capture cross section in the energy range 500 to 750 eV. The circles represent the experimental data of de Saussure *et al*. The solid line is the result of the SAMMY fit including the self-shielding and multiple-scattering effects.
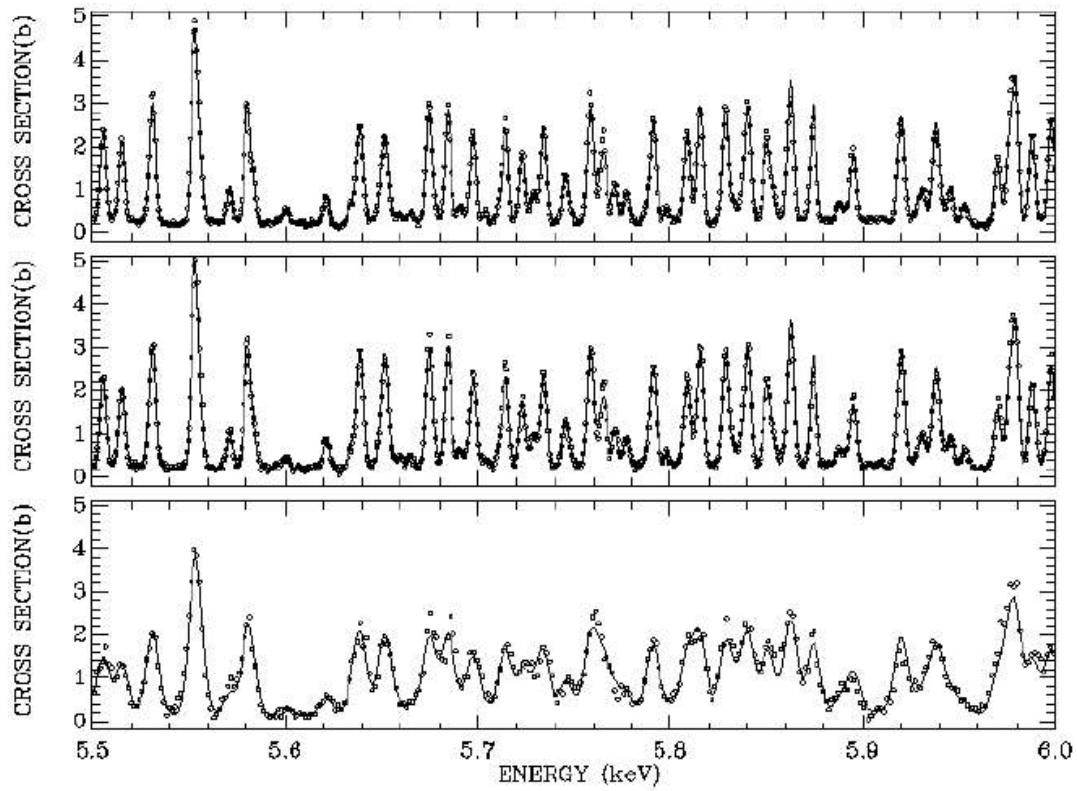
Fig. 12. The neutron effective capture cross section in the energy range 5.5 to 6.0 keV. The circles represent the experimental data of de Saussure *et al*. (lower curve) and of Macklin *et al*. (middle curve and upper curve). The solid lines are the results of the SAMMY fits including self-shielding and multiple scattering effects.

Table 2. Average experimental transmissions, Exp, compared to the values, Theo, calculated with the resonance parameters in the energy range 1 to 20 keV

Energy (keV)	Harvey[3] Thick sample			Harvey[3] Medium sample			Olsen[8] Thick sample		
	Exp.	Theo.	% dev.[a]	Exp.	Theo.	% dev.[a]	Exp.	Theo.	% dev.[a]
1–2	0.1482	0.1482	0.00%	0.5848	0.5846	−0.34%	0.1504	0.1475	−1.97%
2–3	0.1256	0.1247	0.72%	0.5510	0.5586	1.38%	0.1245	0.1242	−0.24%
3–4	0.1138	0.1144	0.53%	0.5408	0.5453	0.83%	0.1138	0.1138	0.00%
4–5	0.1065	0.1075	0.94%	0.5665	0.5716	0.88%	0.1056	0.1069	0.12%
5–6	0.1193	0.1204	0.92%	0.5804	0.5846	0.72%	0.1188	0.1198	0.84%
6–7	0.1198	0.1208	0.83%	0.5616	0.5657	0.73%	0.1179	0.1202	1.95%
7–8	0.1160	0.1162	0.17%	0.5800	0.5838	0.66%	0.1149	0.1157	0.70%
8–9	0.1179	0.1186	0.59%	0.5658	0.5697	0.69%	0.1160	0.1181	1.81%
9–10	0.1171	0.1168	−0.26%	0.5830	0.5856	0.44%	0.1149	0.1161	1.04%
10–11	0.1192	0.1199	0.60%	0.5297	0.5796	−0.02%			
11–12	0.1216	0.1213	−0.25%	0.5831	0.5859	0.48%			
12–13	0.1249	0.1250	0.08%	0.5709	0.5735	0.46%			
13–14	0.1099	0.1097	−0.18%	0.5687	0.5710	0.40%			
14–15	0.1247	0.1244	−0.24%	0.5785	0.5816	0.54%			
15–16	0.1150	0.1152	0.17%	0.5711	0.5747	0.63%			
16–17	0.1205	0.1206	0.08%	0.5848	0.5883	0.60%			
17–18	0.1155	0.1156	0.09%	0.5532	0.5564	0.58%			
18–19	0.0978	0.0970	−0.82%	0.5630	0.5656	0.46%			
19–20	0.1269	0.1260	−0.71%	0.5995	0.6034	0.65%			

[a] Percentage deviation between Theo and Exp.

The final fits in the energy range below 1 keV were performed by allowing the variation of the normalization and the background correction for the two thickest samples and very little variation for the thin samples. The normalization corrections for the two thickest samples, fully correlated to the background correction, were less than 2% at all energies below 1 keV. The average transmission of the two thickest samples are compared to the values calculated with the resonance parameters in Table 3.

Table 3. Average experimental transmissions, Exp, compared to the values, Theo, calculated with the resonance parameters in the energy range 5 to 1000 eV

Energy (eV)	Olsen (0.174 at/b)[7]			Olsen (0.0521 at/b)[7]		
	Exp.	Theo.	% dev.[a]	Exp.	Theo.	% dev.[a]
5–16	0.1655	0.1627	−1.72%	0.5426	0.5456	0.55%
16–60	0.1507	0.1499	−0.53%	0.5029	0.5086	1.13%
60–250	0.1426	0.1424	−0.14%	0.4866	0.4934	1.40%
250–500	0.1203	0.1198	−0.42%	0.5024	0.5096	1.40%
500–750	0.1379	0.1371	−0.58%	0.5084	0.5149	1.28%
750–1000	0.1730	0.1728	−0.12%	0.5274	0.5319	0.85%

[a] Percentage deviation between Theo and Exp.

Due to the quite good consistency of the SAMMY analysis of the transmission data, the accuracy of the calculated average total cross section is about 0.03 b, corresponding to 0.5% accuracy on the thick-sample (0.174-at/b) transmission data. The average neutron elastic cross sections calculated from the present analysis are compared to the values obtained from ENDF/B-VI in Table 4. The ENDF/B-VI values are smaller by 1.5% on average; the difference is mainly due to a different estimation of the effective radius R': 9.48 fm in the present work and 9.43 fm in ENDF/B-VI (Moxon-Sowerby evaluation).

In the SAMMY sequential analysis, the experimental capture data were situated in the last step of the analysis. The most important parameters in the fit of the experimental capture were the background and normalization adjustment parameters, and the parameters for the self-shielding and multiple scattering in the ^{238}U samples. The average capture cross sections inferred by de Saussure *et al.* from their experimental data were much larger than the results of the evaluation performed at the same time (ENDF/B-III or Sowerby evaluation[23]). The average values published by Macklin *et al.*[4] were not corrected for self-shielding and multiple-scattering effects, and could not be compared to any other results. The large background and normalization corrections found by Sowerby and Moxon[1] for the de Saussure data and the Macklin data were confirmed by the present work. In the de Saussure data, the corrections, small at low energy, increase rapidly to about −10% for the normalization and about −50 mb for the background above 100 eV. In the Macklin data, the corrections were about +15 ± 5% for the normalization and −110 ± 30 mb for the background for both samples. However, after these corrections, the experimental data were not compatible with the accuracy published by the authors (5–10% by de Saussure and 8% by Macklin).

Table 4. Average elastic cross sections calculated with the resonance parameters compared to the ENDF/B-VI values

Energy (keV)	Present evaluation (barn)	ENDF/B-VI (barn)
1–2	21.918	21.68
2–3	21.758	21.57
3–4	19.990	19.82
4–5	14.888	14.79
5–6	14.252	14.20
6–7	16.570	16.66
7–8	13.992	13.79
8–9	15.642	15.03
9–10	13.861	13.07
10–11	14.609	14.67
11–12	13.381	14.53
12–13	15.304	14.40
13–14	14.533	14.29
14–15	14.484	14.18
15–16	14.546	14.09
16–17	13.649	14.01
17–18	16.117	13.93
18–19	14.522	13.86
19–20	12.789	13.79

It is unlikely that the background in the capture data could be due to a direct-capture process. A simple estimate of the direct capture at thermal energy is provided by the Lane-Lynn theory.[24] This theory suggested a simple analytical formula for the direct capture of s-wave neutrons to a final p-orbit using spectroscopic factors. For ^{238}U, given the level scheme of ^{239}U, an estimate of 80 mb is obtained. However, with a more rigorous model of direct and semi-direct capture, G. Arbanas[25] demonstrated that the assumptions of the Lane-Lynn theory are not valid in the case of ^{238}U, and that direct capture does not exceed a few millibarn in the energy range of concern for the present evaluation. Consequently, direct capture can be neglected in the present work.

It is important to note that the parameters of the largest resonances were well-defined at the end of the transmission sequences and were not significantly modified by the analysis of the capture data. The capture data were useful for identification and determination of the neutron widths of small resonances not seen in the transmission data, for the accurate determination of the neutron widths of p-wave resonances hidden by the s-wave resonances in the transmission data (mixed multiplets

of *s*- and *p*-wave resonances), and for the determination of the spin of some *p*-wave resonances (see Sect. 5.1).

The calculated average capture cross sections are compared to the ENDF/B-VI values and to the values obtained by de Saussure in Table 5. The values of de Saussure are on average 16% higher, which is consistent with the corrections performed in the present analysis. In the energy range 1 to 10 keV, the ENDF/B-VI values are similar to those obtained in the present evaluation but with a tendency to smaller values above 5 keV. In the energy range 10 to 20 keV, the ENDF/B-VI values are on average 5% larger than the present evaluation. In this energy range the ENDF/B-VI values were due to the Froehner[26] Hauser-Feshbach evaluation in the unresolved-energy range. The Froehner evaluation was a statistical analysis of average total cross sections and capture cross sections in the energy range 10 to 150 keV, mainly based on the experimental data of Kasakov[27] for the capture cross section. The Kasakov experimental data are also given in Table 5; they disagree with the present evaluation by 35% at 5 keV and by 5% on average between 10 and 20 keV. It is likely that part of the large discrepancies encountered among the experimental capture cross sections is due to the inaccuracy of the self-shielding and multiple scattering corrections obtained from poorly determined resonance parameters and to the inadequacy of some computer codes to perform accurate corrections. In the present evaluation, the experimental effects were calculated in the process of fitting the resonances using the latest version of SAMMY, which was widely tested for accuracy of the corrections, particularly via the Monte-Carlo method.[28, 29] See also Figs. 1 and 2.

The average capture cross section calculated by SAMMY from the resonance parameters are generally smaller than those found in the experimental data files. Actually, the calculated values could be too small if there are too many *p*-wave resonances missing from the set of resonance parameters. The SAMMY/URR (unresolved resonance region) statistical analysis[30] of the average total cross section in the energy range 10 to 800 keV gives values of 1.053×10^{-4} and 1.781×10^{-4} for the *s*-wave and *p*-wave neutron strength functions, respectively. As will be shown in the next section, the values calculated from the resonance parameters in the energy range 10 to 20 keV are 1.080×10^{-4} and 1.715×10^{-4}, respectively, and about half of the capture cross section is due to the contribution of the *p*-wave neutrons. Comparison with the Porter-Thomas distribution (see next section) shows that only the very small *p*-wave resonances were not taken into account in the SAMMY analysis; the missing *p*-wave resonances could contribute to only 0.4 % of the strength function, corresponding to about 1.5 mb in the capture cross section, which cannot explain the difference of about 5% (~25 mb) between Kasakov (ENDF/B-VI) and the present results in the energy range 10 to 20 keV. An effect of wrong spin assignments could also exist (too many resonances of spin $J = 1/2$). Changing all the resonances with spin $J = 1/2$ to resonances with spin $J = 3/2$ increases the average capture cross section by 6% in the energy range 10 to 20 keV. A more realistic change, concerning only few resonances, could increase the cross section by not more than 1 to 2%. The present evaluation shows definitively that, at least in the energy range thermal to 20 keV, the ^{238}U capture cross section is smaller than most of the available experimental data, in which discrepancies as large as 30% could be found. The average capture cross sections calculated with the present resonance parameters have an accuracy of about 3%.

Table 5. **Average capture cross sections (barns) calculated with the resonance parameters compared to the ENDF/B-VI values and to other experimental data**

Energy keV	Present values	de Saussure[12]	ENDF/B-VI	Moxon[31]	Kasakov[27]
1–2	1.868	2.12	1.87	1.95	
2–3	1.362	1.56	1.36	1.45	
3–4	1.149	1.31	1.15	1.23	
4–5	0.855	1.02	0.88	0.964	1.154
5–6	0.861	1.02	0.90	0.940	1.155
5–7	0.840	1.00	0.87	0.824	0.881
7–8	0.741	0.862	0.68	0.793	0.850
8–9	0.650	0.772	0.63	0.723	0.767
9–10	0.702	0.764	0.65	0.722	0.738
10–11	0.676		0.71		
11–12	0.643		0.68		
12–13	0.621		0.66		
13–14	0.676		0.64		
14–15	0.588		0.62		
15–16	0.560		0.60		
16–17	0.550		0.58		
17–18	0.559		0.57		
18–19	0.517		0.55		
19–20	0.479		0.54		
10–20	0.587	0.688	0.615	0.612	0.617

5. RESULTS OF THE ANALYSIS: THE RESONANCE PARAMETERS

5.1. GENERALITIES

The ^{238}U nucleus has spin and parity $I^\pi = 0^+$. The neutron resonances are induced via one channel spin $s = 1/2$. The spin of the s-wave resonances (neutrons of angular momentum $l = 0$) is $J^\pi = 1/2^+$, and the spins of the p-wave resonances (neutrons of angular momentum $l = 1$) are $J^\pi = 1/2^-$ and $J^\pi = 3/2^-$. The $l = 1$ and $l = 2$ neutron penetrability factors relative to $l = 0$ are given in Table 6. Due to the rather large value of the s-wave resonance average spacing and to the good statistical accuracy of the Olsen thick-sample transmission data, very small resonances can be observed in the experimental data at low energy; most of these resonances are p-wave resonances. Other small p-wave resonances are seen in the experimental capture data and not in the transmission data. In the energy range above 10 keV, some observed small resonances could be d-wave resonances ($l = 2$); however, the existing experimental data do not allow distinction between p-wave resonances and d-wave resonances. In the present analysis only s-wave and p-wave resonances were used to fit the experimental data.

Table 6. Penetrability factors for p-wave, P_1, and d-wave, P_2, neutrons relative to s-wave neutrons

Neutron energy (eV)	ka	P_1	P_2
0.001	0.0021	0.4296×10^{-5}	0.2051×10^{-11}
0.100	0.0207	0.4295×10^{-3}	0.2051×10^{-7}
1.000	0.0655	0.4278×10^{-2}	0.2048×10^{-5}
10.000	0.2073	0.4119×10^{-1}	0.2022×10^{-3}
20.000	0.2931	0.7913×10^{-1}	0.7969×10^{-3}

ka = $0.00220E^{1/2}$a, where E = neutron energy in eV, and a = nuclear radius in 10^{-12} cm.

The identification of the largest s-wave resonances is straightforward, involving the asymmetry of the cross section due to the potential-resonant interference effect. All the resonances which cannot be identified as s-wave resonances had to be distributed among three families: small s-wave resonances, $J = 1/2$ p-wave resonances, and $J = 3/2$ p-wave resonances.

In some cases it has been possible to assign the spin $J = 1/2$ or $J = 3/2$ from the area of the resonance in the capture cross section. In the single-level Breit-Wigner approximation, the capture area of an isolated resonance is proportional to $g\Gamma_n \Gamma_\gamma/\Gamma$, with $\Gamma = \Gamma_n + \Gamma_\gamma$; $g\Gamma_n$ is known from the analysis of the transmission data. If $g\Gamma_n = A$, the ratio of the capture area calculated with $g = 2$ (spin $J = 3/2$) to the capture area calculated with $g = 1$ (spin J = 1/2) is $2(A+\Gamma_\gamma)/(A+2\Gamma_\gamma)$. The

ratio varies from 1 to 2 for A varying from extremely small values to extremely large values. At low energy, the Γ_n values of the p-wave resonances are very small, and dependance on the spin of the capture area is not seen. When the neutron energy increases, Γ_n increases to values of the same order of magnitude as Γ_γ, and the spin effect could be important.

As an example, Fig. 13 shows the results of the calculation in the energy range from 5.4 to 5.6 keV. The upper part of the figure shows the capture cross section calculated from the current resonance parameters with $g\,\Gamma_n$ values obtained from the SAMMY fit of the transmission data. In the middle part, the same values of $g\,\Gamma_n$ were used, but the spins of the p-wave resonances were changed from $J = 1/2$ to $J = 3/2$ or from $J = 3/2$ to $J = 1/2$, resulting in a bad representation of six resonances (those marked by the letter S on the figure). Another good fit of the capture cross section could be obtained from SAMMY by allowing the variation of Γ_n, as shown in the lower part of the figure, but the new values of Γ_n will not be consistent with the experimental transmission data.

Another example is shown in Fig. 14 in the energy range from 16.0 to 16.3 keV, where the overlap of the resonances is much more important. The adopted spin assignments allow a reasonably good representation of the cross section (upper part of the figure); changing the spin of the large p-wave resonances while keeping the same $g\,\Gamma_n$ values results in a bad representation of the cross section (lower part of the figure).

Two other sources of spin assignments were used in the present work: those of Corvi, Rohr, and Weigmann[32] and those of Gunsing et al.[33] These spin assignments were also used by Crawford et al.[34] for their study of parity nonconservation.

According to the $2J+1$ law of the level density dependance, the number of $J = 1/2$ p-wave resonances should be approximately the same as the number of s-wave resonances; the number of the $J = 3/2$ p-wave resonances should be twice this number. However, complete sets of resonances can never be obtained from experimental data because (1) resonances with very small values of neutron width are not seen in the experimental data, and (2) as energy increases it becomes more difficult to separate overlapping resonances, due to the increase of the resolution and Doppler broadening widths with energy. In order to obtain a complete set of resonances of a given spin, it is assumed that the reduced neutron widths obey a Porter-Thomas distribution[35] and that the level spacings obey a Wigner distribution.[36]
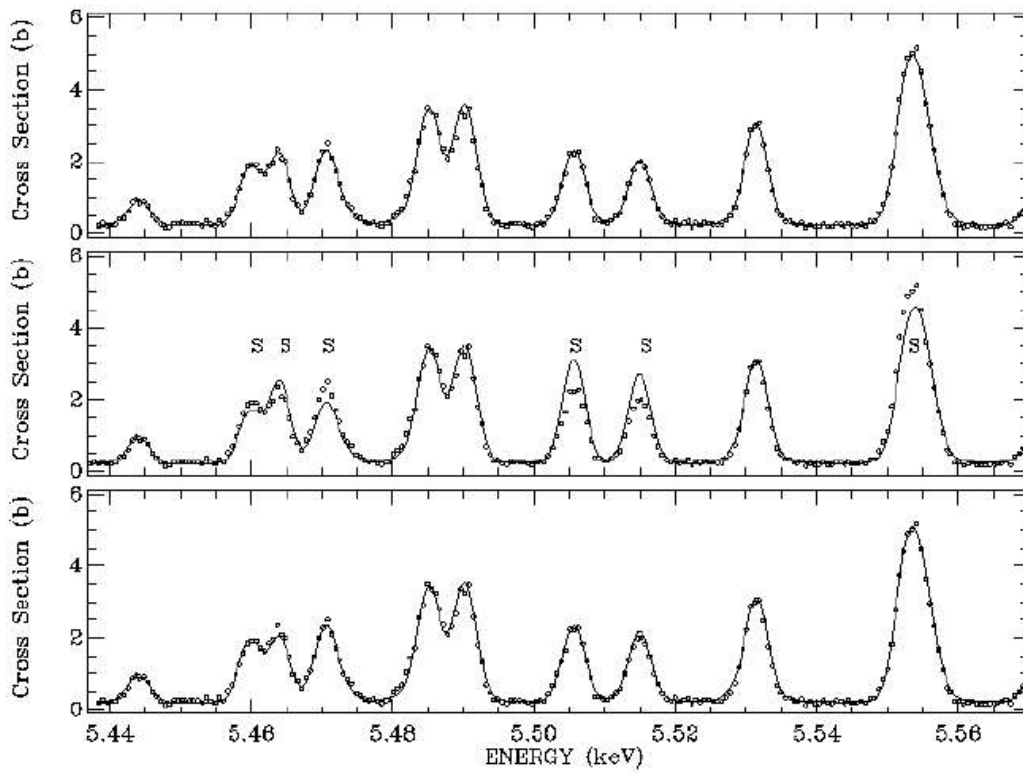
Fig. 13. Example of spin assignments from the capture area of the resonances.
The circles represent the thin-sample experimental capture data of Macklin *et al*. The solid
lines are the results of the SAMMY calculations with the current resonance parameters (upper
curve), with spin change for six *p*-wave resonances marked with the letter S (middle curve),
and with the neutron widths obtained from a refit of the data (lower curve).
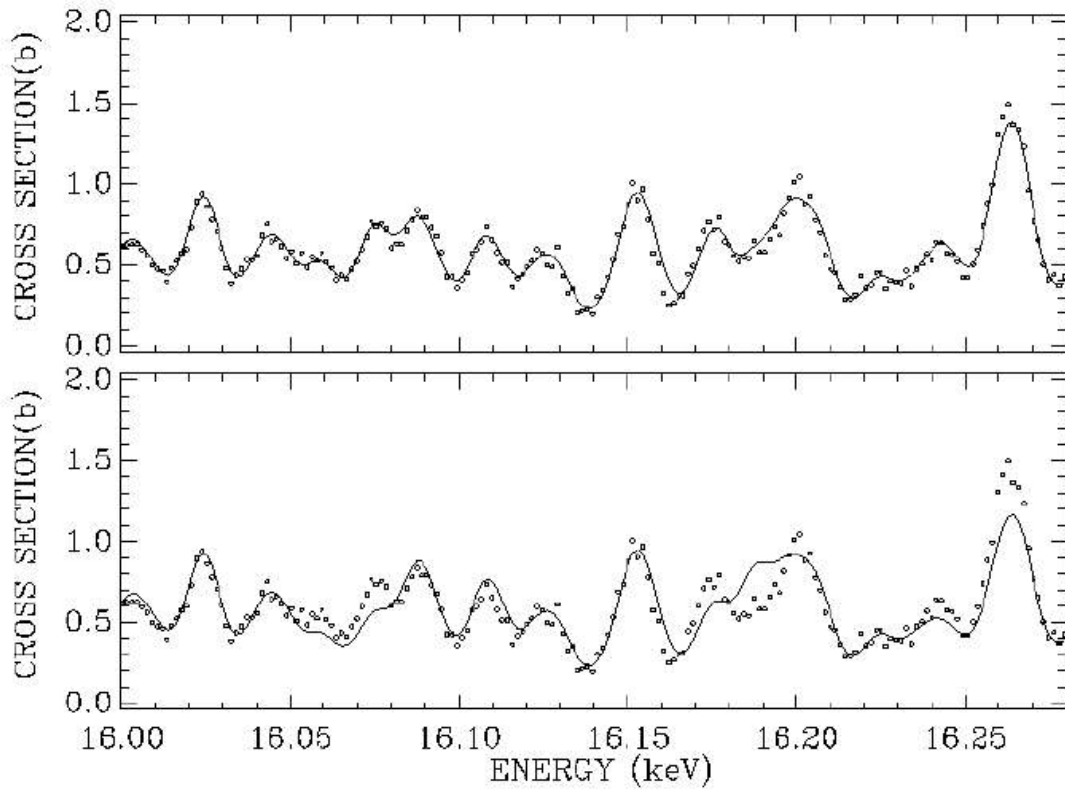
Fig. 14. Example of spin assignments from the capture area of the resonances.
The circles represent the thin-sample experimental data of Macklin *et al*. The solid lines are the results of the SAMMY calculations with the current resonance parameters (upper curve), and with spin change for the large *p*-wave resonances (lower curves).

The ^{238}U resonance parameters of ENDF/B-VI, which were used as prior values in the present SAMMY analysis, were consistent with the Porter-Thomas and Wigner distributions, at least for the *s*-wave resonances, as is shown in Figs. 15 and 16 for the reduced neutron widths. This agreement was obtained by Sowerby and Moxon by adding (with the help of the Δ_3 statistics) small or very small resonances to the set of observed resonances. Most of these small resonances were kept in the present analysis. In the energy range 10 to 20 keV, where the current analysis was started from scratch, a large number of non-observed small resonances were also added to the set of observed resonances.
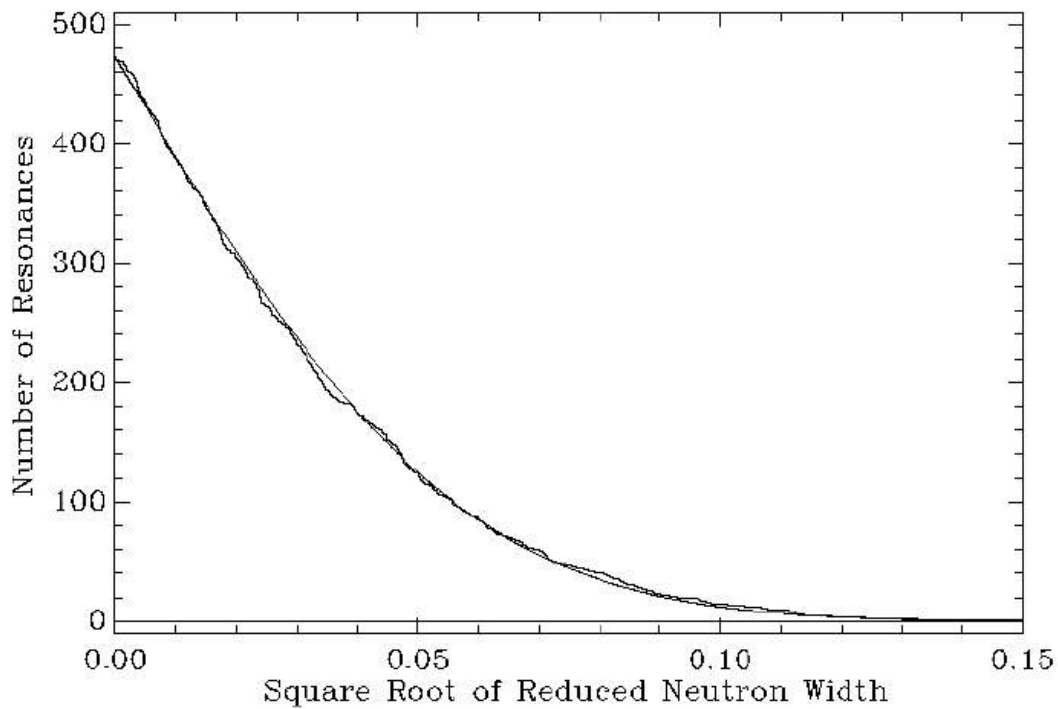
Fig. 15. Integral distribution of the *s*-wave reduced neutron widths of the ENDF/B-VI ^{238}U resonance parameters. The histogram represents the variation of the number of resonances for which the reduced neutron width is larger than the abscissa $(\Gamma_n^0)^{1/2}$. The solid line is the Porter-Thomas distribution normalized to the same number of resonances.
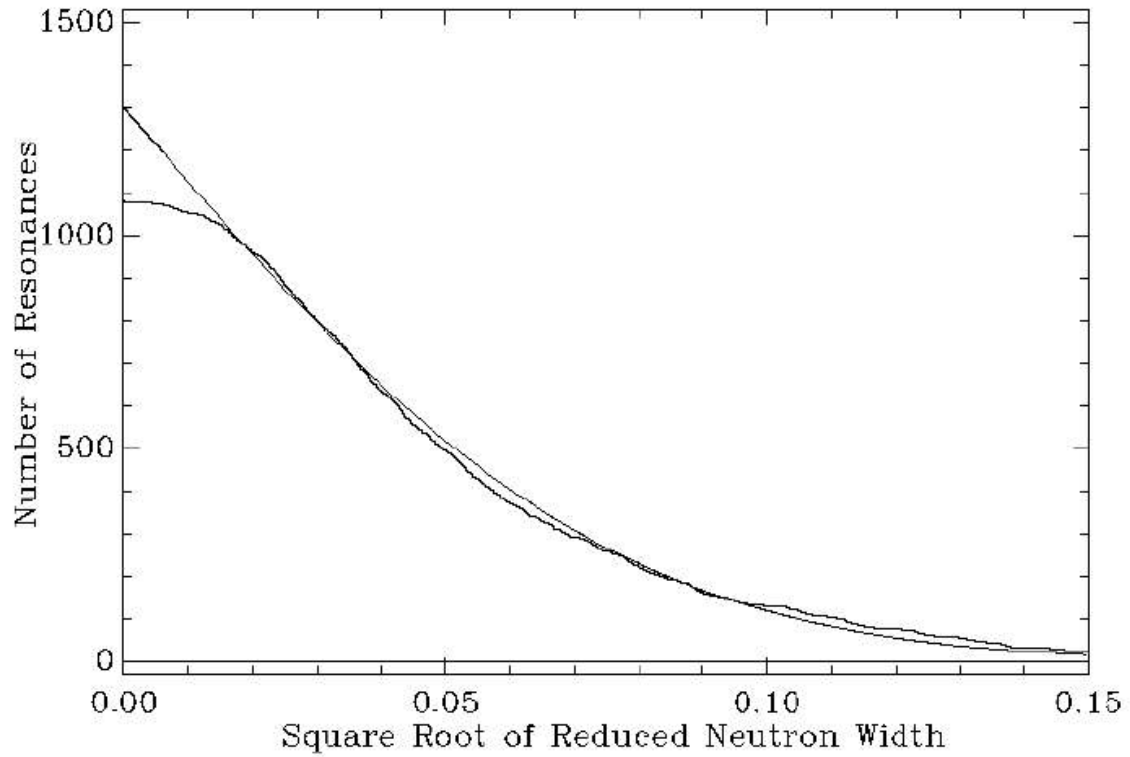
Fig. 16. Integral distribution of the *p*-wave reduced neutron widths of the ENDF/B-VI [238]U resonance parameters. The histogram represents the variation of the number of resonances for which the reduced neutron width is larger than the abscissa $(g\Gamma_n^1)^{1/2}$. The solid line is the Porter-Thomas distribution normalized to a number of 1300 resonances. About 15% of resonances (small resonances) are still missing in the data set.

A total of 3343 resonances were used for the description of the experimental data in the energy range from thermal to 20 keV. This number includes two large fictitious resonances at energies -4400 eV and 24400 eV, which were used to simulate the contribution of the s-wave negative-energy resonances below -500 eV and of the s-wave resonances above 4200 eV. It also includes a ladder of resonances in the energy range -500 to 0 eV, with a constant spacing of 20 eV; this ladder was adopted from the ladder used in ENDF/B-VI file. A small resonance at -7 eV was added in order to fit the Poenitz measurement of the thermal capture cross section.[13] The resonances between 20 and 20.2 keV were those obtained from a crude analysis of the Harvey experimental transmission. The number of resonances versus neutron energy is given in Fig. 17, for both s- and p-wave resonances. In the energy range 0 to 20 keV, there are 898 s-wave, 849 p-wave ($J = 1/2$), and 1565 p-wave ($J = 3/2$) resonances, with average spacing of 22.27, 23.56, and 12.78 eV, respectively, corresponding approximately to the ($2J + 1$) spin dependance of the nuclear level density.
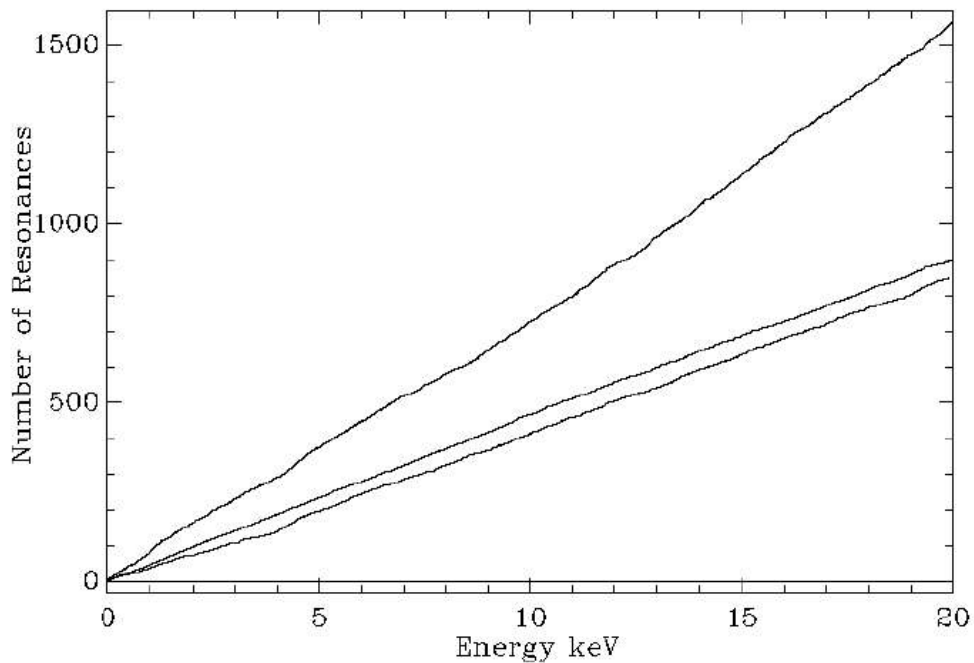
Fig. 17. Variation of the number of resonances versus neutron energy in the neutron energy range 0 to 20 keV for the s-wave resonances (middle curve), the $J = 1/2$ (lower curve) and the $J = 3/2$ (upper curve) p-wave resonances.

It should be stressed that this entire set of resonance parameters should not be used for a statistical study or for determination of average resonance parameters, since the set contains a large number of resonances not seen in the experimental data. The unseen resonances were randomly added in order to conform as much as possible with the Wigner distribution of level spacings and with the Porter-Thomas distribution of reduced neutron widths. As described above, completing the set of observed resonances was needed in order to minimize the effect of the missed levels on the calculation of the average cross sections, particularly the capture cross section.

The distributions of the parameters are given in Figs. 18–21. Assuming the set of *s*-wave resonances is fairly complete, the set of *p*-wave resonances still appears to be missing about 15% of the resonances (very small resonances). These, however, have very little effect on the accuracy of the calculated capture cross section.
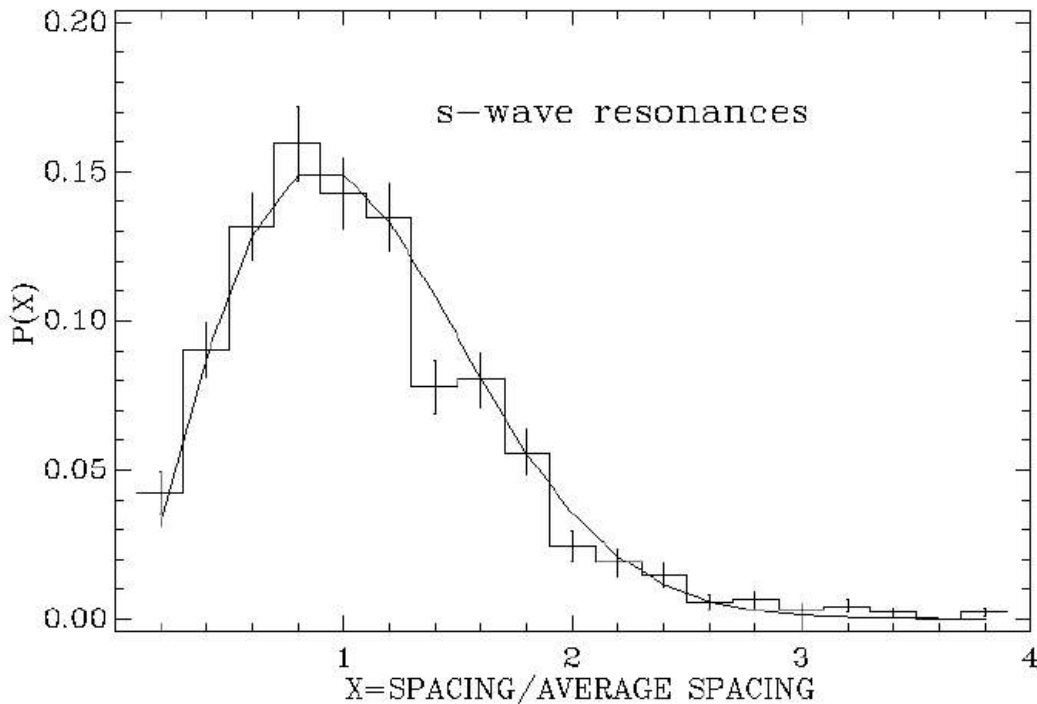
Fig. 18. The level spacing distribution for the *s*-wave resonances in the neutron energy range 0 to 20 keV. The histogram represents the experimental data and the solid line is the Wigner distribution.
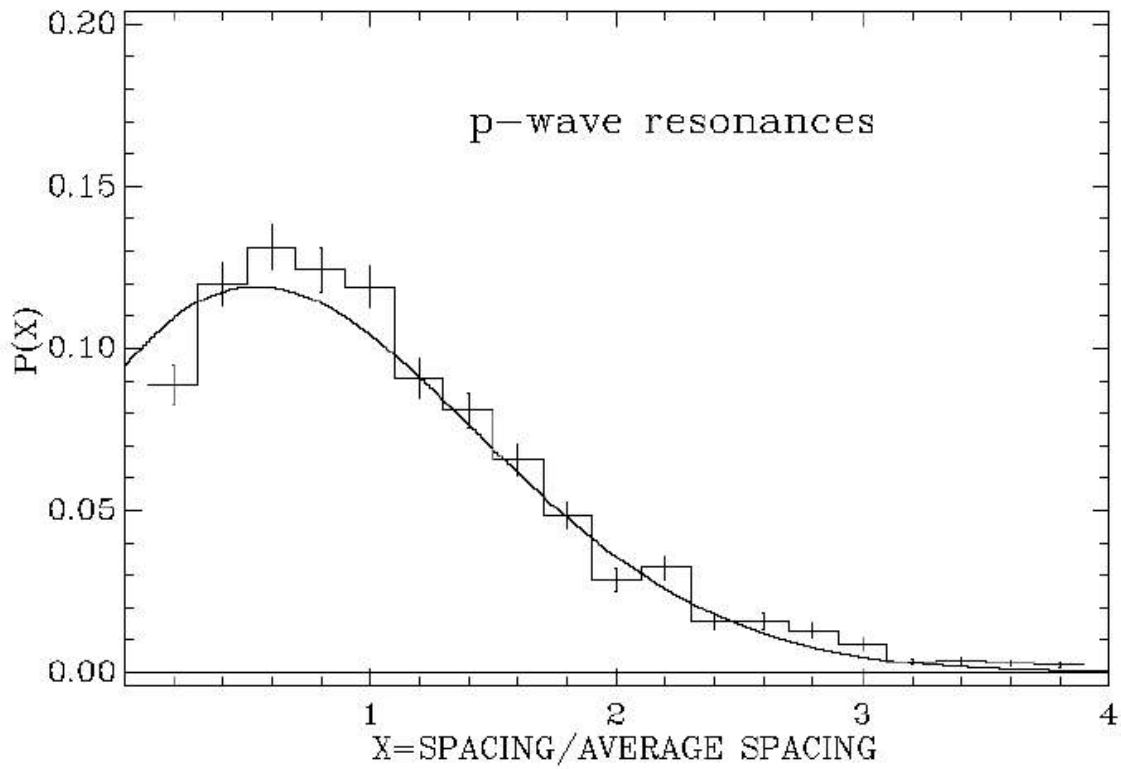
Fig. 19. The level spacing distribution of the *p*-wave resonances in the neutron energy range 0 to 20 keV. The histogram represents the experimental data. The solid line is the theoretical distribution corresponding to two uncorrelated Wigner distributions in the ratio of the population of the two *p*-wave spins.
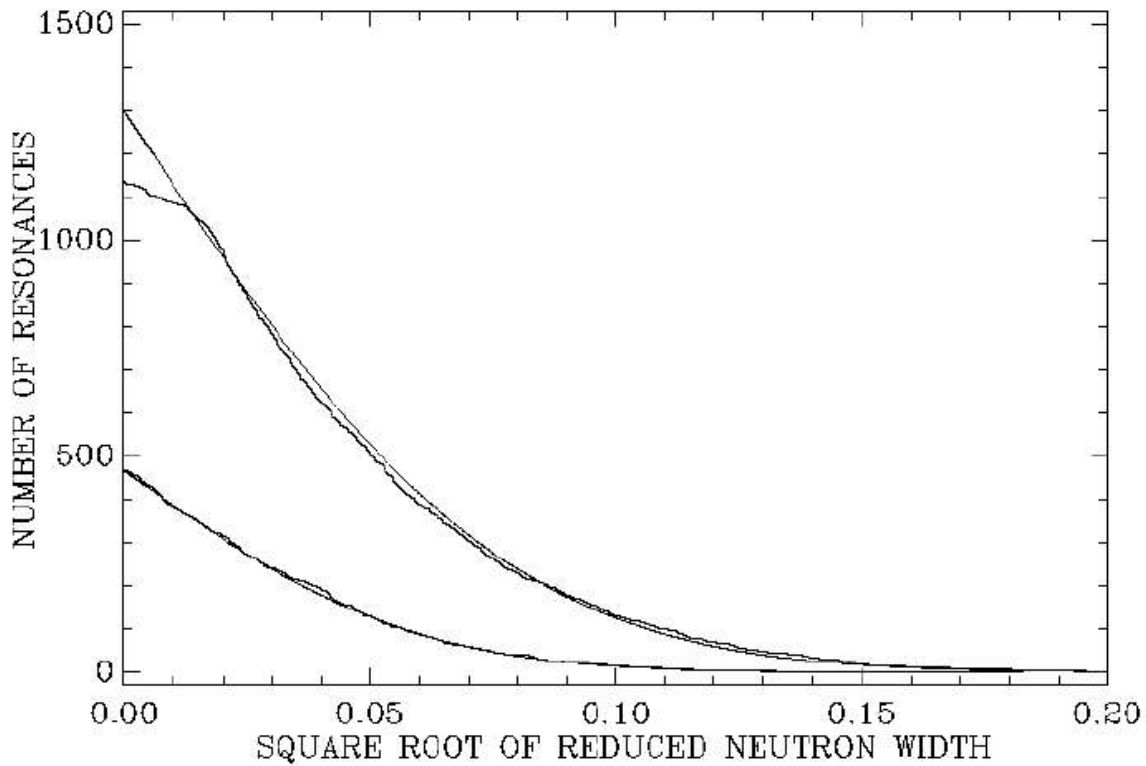
Fig. 20. Integral distributions of the reduced neutron widths in the energy range 0 to 10 keV for the *s*-wave resonances (lower curve) and the *p*-wave resonances (upper curve). The solid lines are the Porter-Thomas distribution normalized to the number of resonances, showing that the sample of *s*-wave resonances is complete, when the *p*-wave sample still indicates that about 15% of the very small resonances are missed.
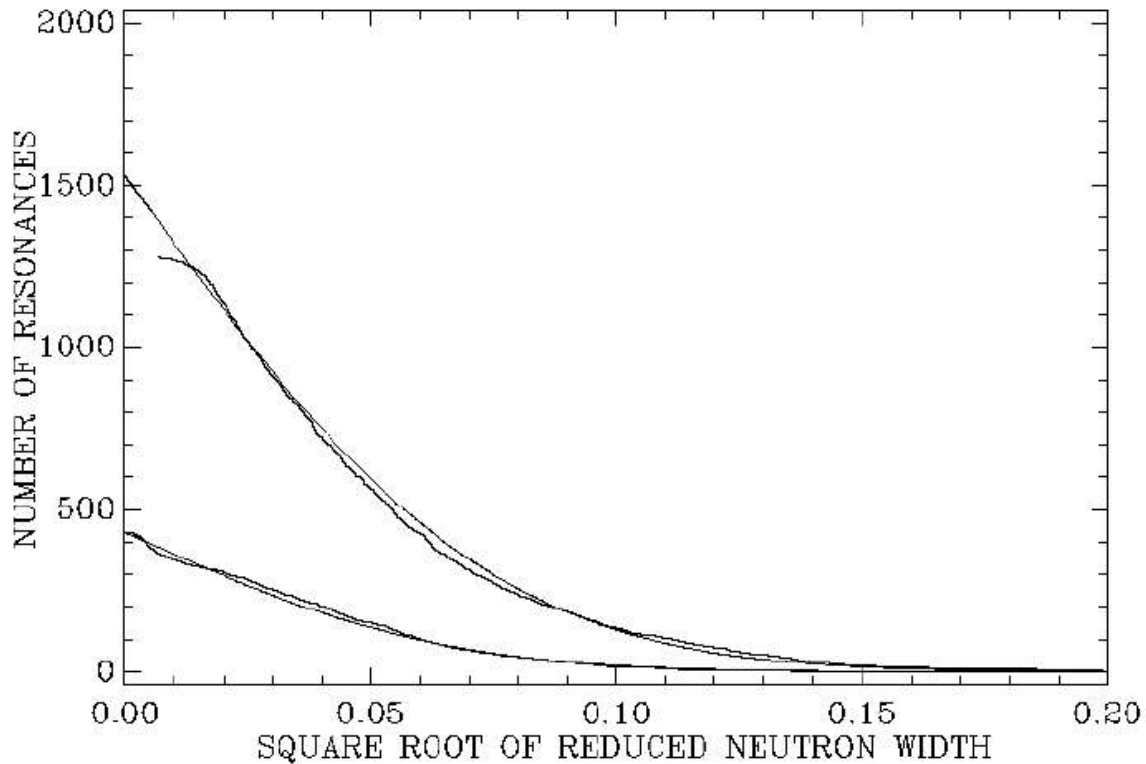
Fig. 21. Integral distributions of the reduced neutron widths in the energy range 10 to 20 keV for the *s*-wave resonances (lower curve) and the *p*-wave resonances (upper curve). The solid lines are the Porter-Thomas distribution normalized to the number of resonances. The deviation between the experimental and the theoretical distributions is more important than in the energy range 0 to 10 keV (Fig. 20), mainly because of the difficulties of fitting the unresolved multiplets in the experimental transmission and capture data.

After 1963 but prior to the important measurements undertaken at ORELA, ^{238}U resonance parameters were obtained by several authors from analyses of numerous transmission and capture measurements.[37–44] Comparisons among those results can be found in the 1977 publication by Olsen *et al.*[7] and in the proceedings of the 1975 Brookhaven National Laboratory seminar on ^{238}U resonance capture.[45]

5.2. RESONANCE PARAMETERS IN THE LOW-NEUTRON-ENERGY RANGE

The energy range below 1 keV is particularly important for calculations for thermal reactors and needs to be treated with great care. The thermal capture value was recently evaluated by Trkov *et al.*[46] from all the available experimental data. His recommended value of 2.683 b is almost the same as the Poenitz experimental result used in the present SAMMY analysis. Readjusting the cross section to the exact Trkov-recommended value could be easily done by modifying the parameters of the fictitious resonance at -7 eV. The calculated capture cross section has the 1/v shape in the thermal energy range, as shown in Fig. 22 along with the Corvi experimental data. The calculated scattering cross section is 9.280 b, close to the average value deduced from bound coherent scattering length measurements (Table 7).[47–51] An important part of the thermal cross sections is determined by the bound level parameters (simulated by the negative resonances) and by the effective scattering radius R′. The present thermal cross sections are significantly smaller than the ENDF/B-VI values of 2.717 b for the capture and 9.360 b for the scattering. The smaller value of the scattering cross section was obtained by decreasing the neutron widths of the negative resonances in the energy range -30 to -500 eV (local strength function of 1.17×10^{-4} in ENDF/B-VI and 0.80×10^{-4} in the present analysis).

The parameters of the *s*-wave resonances at 6.7, 20.8, and 36.6 eV were obtained by fitting the seven transmission measurements of Olsen, the four room-temperature transmission measurements of Meister, and the capture measurement of de Saussure. Special attention was paid to the modeling of the Doppler broadening to take into account chemical binding in metallic and oxide samples. As discussed elsewhere,[52] the CLM of SAMMY (which explicitly accounts for phonon creation and absorption in the atomic lattice) was used to describe the shape of the 6.67-eV resonance. Compared with the traditional approach using the FGM and a fitted effective temperature, the effect of the CLM on the neutron and radiation widths was found to be small. To get a better correction of errors in normalization and backgrounds, the fits were performed resonance by resonance up to 60 eV. An example of these fits is given in Fig. 23.

The parameters of the first *s*-wave resonances, mainly determined by the thickest-sample transmission data of Olsen, are displayed in Table 8. For the important 6.67-eV resonance, the radiation width analyzed with the CLM is very close to the Sowerby-Moxon value, while the neutron width is smaller by 1.2%. For other *s*-wave resonances below 102 eV, the Γ_γ extracted are on average 0.7% higher than those deduced by Sowerby and Moxon from the same data. This can be explained by the use of a different value for the effective scattering radius R′, which modifies the shape of the calculated total cross section in the wing of the resonances. In the final fits in the energy range below 1 keV, values for Γ_γ were obtained for the 31 *s*-wave resonances; the average

value was 23.24 meV (from 16 resonances) in the energy range thermal to 500 eV, and 23.21 meV (from 15 resonances) above 500 eV.
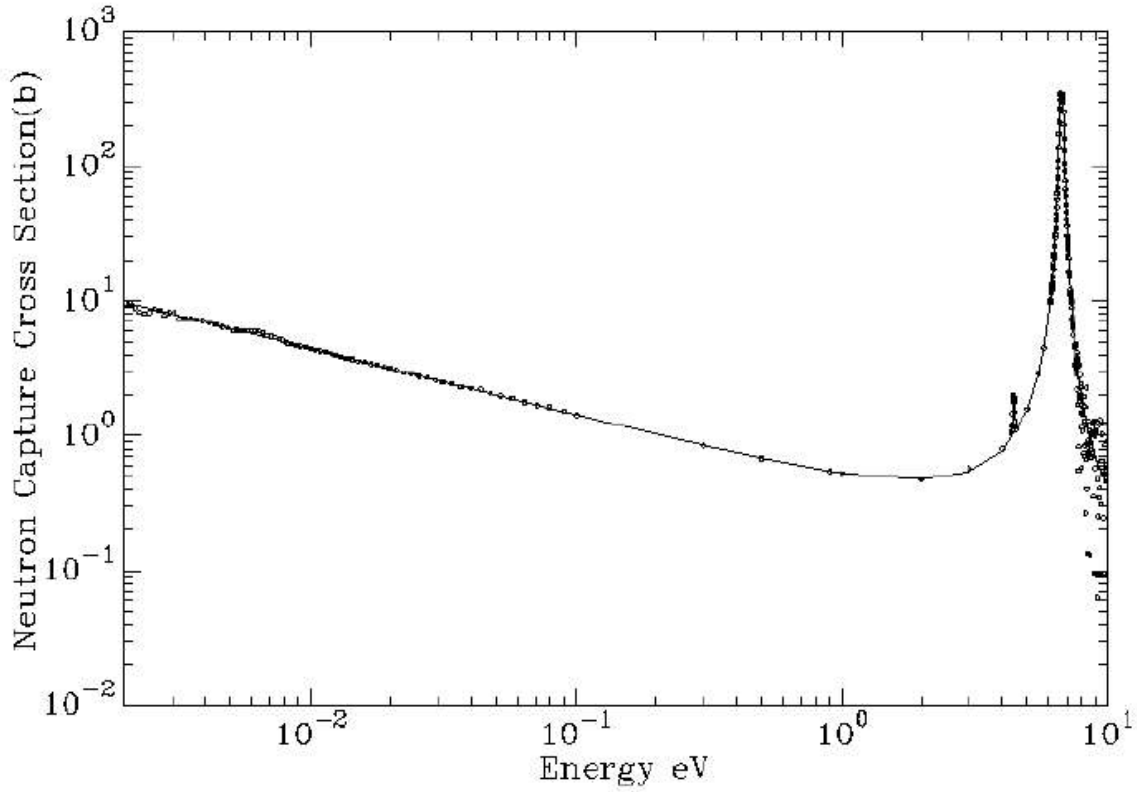
Fig. 22. The capture cross section in the thermal energy range. The circles represent the experimental data of Corvi *et al*. in the energy range below 0.1 eV, normalized at 0.0253 eV, and the de Saussure data above 4 eV. The solid line represents the results of the SAMMY calculations with the resonance parameters.

Table 7. The scattering cross section at 0.0253 eV

Reference	Coherent scattering length b(fm)	Scattering cross section $\sigma_n(b)$
Atoji *et al.* (1961)[47]	8.55 ± 0.06	9.38
Roof *et al.* (1962)[48]	8.4 ± 0.2	9.06
Willis *et al.* (1963)[49]	8.50 ± 0.06	9.27
Koestler (1974)[50]	8.63 ± 0.04	9.56
Mughabghab[16]	8.55 ± 0.04	9.38
Boeuf *et al.* (1982)[51]	8.407 ± 0.007	9.08
Present value		9.28

$\sigma_n = 4\pi a^2$
$b = [A/(A+1)]a + Zb_{ne}$
$b_{ne} = -(1.38 \pm 0.3) \times 10^{-3}$
A = atomic mass
Z = atomic number
b_{ne} = neutron-electron interaction length
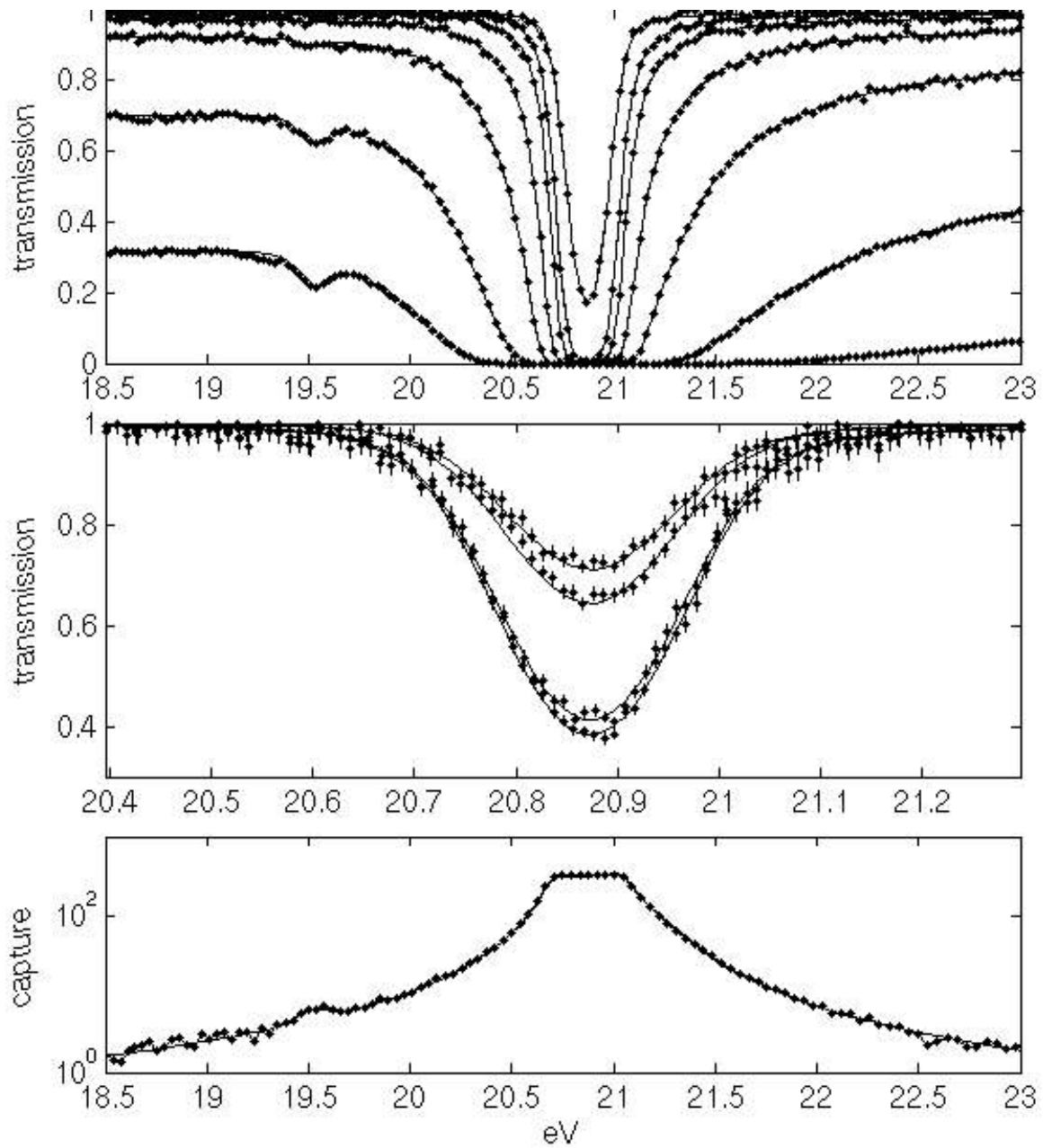
Fig. 23. The resonance at 20.9 eV. The Olsen *et al*. experimental transmission data are shown on the upper part of the figure, the Meister *et al*. transmission data in the middle part, and the de Saussure capture data at the lower part. The solid lines represent the corresponding data calculated with the resonance parameters.

**Table 8. The *s-wave* resonance parameters of ^{238}U in the
neutron energy range 0 to 105 eV**

Energy (eV)	Present work		Sowerby-Moxon[1]	
	Γ_γ	Γ_n	Γ_γ	Γ_n
6.673	23.00	1.476	23.00	1.493
20.872	22.86	10.09	22.91	10.26
36.682	23.00	33.55	22.89	34.13
66.031	23.31	24.18	23.36	24.60
80.747	23.39	1.874	23.00	1.865
102.569	24.08	70.77	23.40	71.70

The widths Γ_γ and Γ_n are given in meV.

For comparison with other results, the reader is referred to the comprehensive review of the capture widths of the low-energy *s*-wave resonances made by Olsen *et al.*[7] For the low-energy *p*-wave resonances, the neutron widths are very small and the capture areas are very close to the total area. The $J = 3/2$ *p*-wave at 10.239 eV is well defined in the thick-sample transmission data of Olsen. The capture width of this resonance is nearly equal to the total width and can be obtained from the shape analysis of the thick-sample transmission data; the SAMMY fit to the transmission and the capture data give a value for Γ_γ of 21.3 ± 1.6 meV; the error takes into account a 2% error on the effective temperature of the samples. The result of the SAMMY fit is shown in Fig. 24. The *p*-wave resonances at 83.71, 263.98, and 454.14 were also analyzed individually and values of 21.01, 20.06, and 19.94 meV were obtained for Γ_γ, respectively, with a large error of about 20% due to the fact that the shape of these resonances is not very sensitive to the capture width [the combination of Doppler and resolution broadening is larger than 350 meV FWHM (full width half maximum) at the corresponding energies].

The capture resonance integrals at infinite dilution are compared to ENDF/B-VI values in several energy ranges in Table 9.
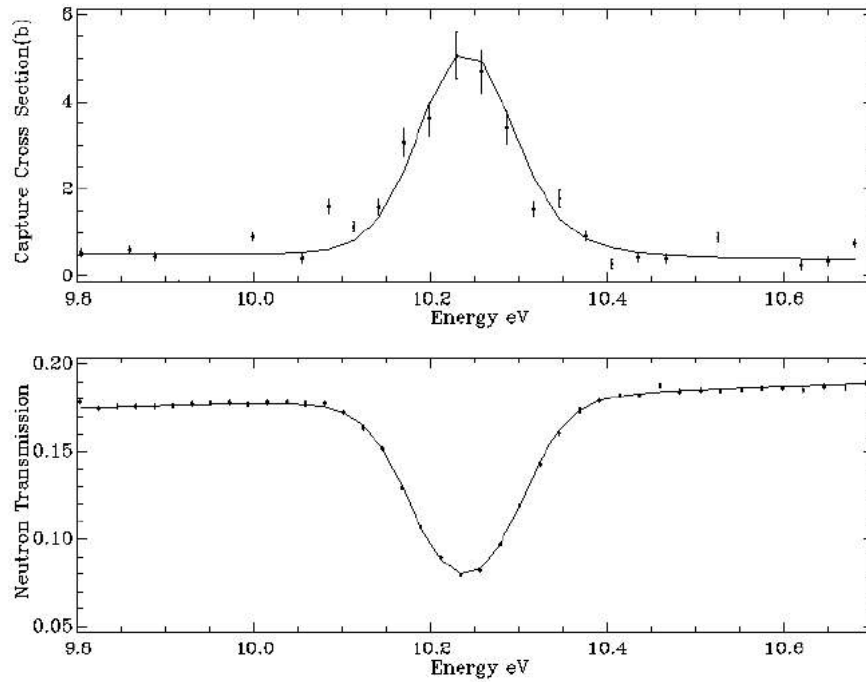
Fig. 24. The *p*-wave resonance at 10.239 eV. The de Saussure capture data are shown in the upper part of the figure and the Olsen thick sample transmission data in the lower part. The solid lines represent the corresponding values calculated with the resonance parameters.

Table 9. Capture infinite-dilution resonance integrals; present values and ENDF/B-VI values

Energy range (eV)	Present values (barn)	ENDF/B-VI (barn)	Difference
0.01–0.1	5.85	5.93	1.2%
0.1–1.0	2.47	2.51	1.5%
1.0–6.0	1.74	1.77	1.6%
6.0–10.0	127.56	128.94	1.1%
10.0–25.0	66.35	67.22	1.3%
25.0–50.0	41.84	42.13	0.7%
50.0–100.0	12.52	12.57	0.4%
0.5–10000	271.33	274.01	1.0%

5.3. AVERAGE LEVEL SPACING

The average level density is an important nuclear parameter used in model calculations of neutron cross sections at different excitation energies. The level density is measurable in the neutron cross section resolved-resonance region by counting the number of levels seen in a given neutron energy range in data obtained with good experimental resolution. This gives a reference point at an excitation energy equal to the neutron binding energy in the excited compound nucleus; another point could be obtained by the study of low-lying excited levels, accessible by gamma ray spectroscopy, for instance.

In this study, the *s*-wave average level spacing, corresponding to the 898 *s*-wave resonances used to fit the experimental data in the neutron energy range 0 to 20 keV, is 22.30 eV. As discussed above, this does not correspond to an observed experimental value because many small levels, not seen in the experimental data, were randomly added to the set of observed resonances in order to improve agreement with the theoretical distribution. Furthermore, due to the increase of the Doppler- and experimental-resolution widths with increasing energy, an increasing number of multiplets of several resonances is observed as neutron energy increases. Because the choice of representation for the multiplets is far from unique, an important bias could be introduced in the analysis. It is likely that better estimation of the average level spacing would be obtained from a sample of smaller size in a lower energy range.

The distribution of the reduced neutron widths of the sample of *s*-wave resonances in the energy range 0 to 2500 eV is given in Fig. 25. This sample contains only the 93 observed resonances which have greater than 99% probability to be *s*-wave resonances. Below 2500 eV, the probability of finding unresolved multiplets is very small. The experimental distribution can be fitted by a Porter-Thomas distribution, assuming that all the resonances with Γ^0_n smaller than 0.20 meV are missing in the sample; the lower estimation of the number of missing levels is 22 and the higher estimation is 27, corresponding to average level spacing of $D_0 = (21.19 \pm 0.55)$ eV. This value is significantly smaller than the value of (23.0 ± 0.6) eV recommended by Froehner[26] from a statistical analysis of the average cross section in the unresolved energy range, and also smaller than the value of (22.5 ± 0.8) found by the same author from the statistical analysis of JEF-2 data in the energy range 0 to 4 keV. A more comprehensive study[53] of the statistical properties of the ^{238}U resonance parameters of the present evaluation, using several methods for extracting the average level density, confirms the present small value of the *s*-wave level spacing.
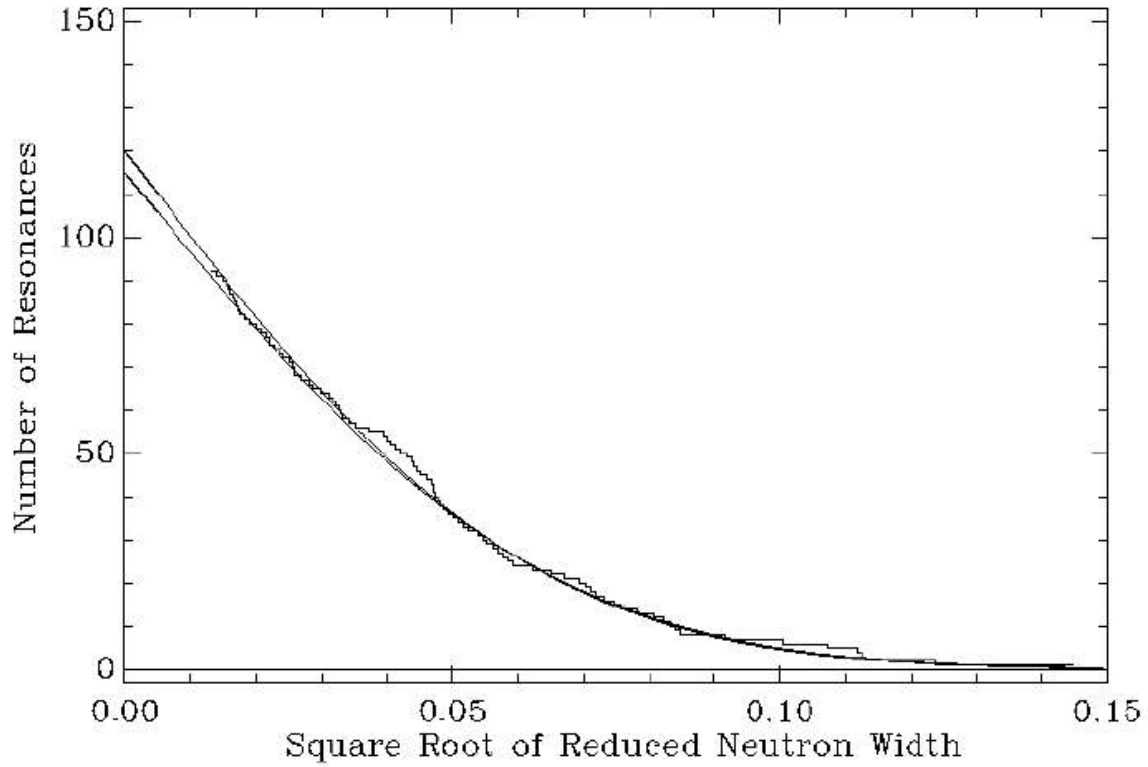
Fig. 25. Integral distribution of the reduced neutron widths of the *s*-wave resonances for the neutron energy interval 0 to 2500 eV. The sample contains only the 93 observed resonances with a 99% probability of being *s*-wave resonances. The two solid lines represent the Porter-Thomas distribution normalized to 115 and 120 number of resonances, respectively, taking into account 22 or 27 nonobservable small resonances.

47

5.4. REDUCED NEUTRON WIDTHS AND NEUTRON STRENGTH FUNCTIONS

The reduced neutron width and the neutron strength function are generally obtained by using the following relations:

$$\Gamma^0_n = \Gamma_n/E^{1/2} \qquad \text{(s-wave resonances)}$$
$$\Gamma^l_n = (\Gamma_n/E^{1/2})(1+P) \qquad \text{(p-wave resonances)}$$
$$S_l = [1/(2l+1)\Delta E]\Sigma g\Gamma^l_n \qquad \text{(strength function of angular momentum } l\text{)}$$

with $P = 1/k^2a^2$ and $a = 1.23A^{1/3}+0.8$ fm

where Γ^l_n is the reduced neutron width of a resonance of angular momentum l, a the nuclear radius, and A the atomic mass. The energy interval ΔE containing the resonances of the corresponding sample is taken as the difference between the energy of the last resonance and the energy of the first resonance plus one average spacing.

Histograms of the cumulative sum of the reduced neutron widths $g\Gamma^l_n$, versus neutron energy, for all the resonances assigned s and p in the energy range 0 to 20 keV, are given in Fig. 26. The strength functions, as defined by the above relations, correspond to the slope of the histograms and are $S_0 = (1.025 \pm 0.047) \times 10^{-4}$ and $S_1 = (1.652 \pm 0.046) \times 10^{-4}$, respectively. The errors are the sampling errors $(2/n)^{1/2}$, where n is the number of resonances in the sample. These values are not too sensitive to the small resonances, which could still be missing, or to the manner of distributing the resonances in the experimentally unresolved multiplets of the high-energy range, because the SAMMY shape analysis allows the accurate description of the total area of the multiplets. That is, the sum of the $g\Gamma^l_n$ of a multiplet does not depend too much on the number of resonances used to represent the multiplet. The value of S_1 is significantly smaller than the value of 2.0×10^{-4} obtained by Froehner[26] from the statistical analysis of the average cross section in the energy range above 10 keV. However, the SAMMY/URR statistical model fit[53] of the average total cross sections obtained from the Harvey high-resolution transmission data[54] gives a value of 1.78×10^{-4} in the energy range 10 to 100 keV, with $S_0 = 1.053 \times 10^{-4}$ and $R' = 9.44$ fm. A low S_1 value of $(1.68 \pm 0.28) \times 10^{-4}$ was also obtained by Tsubone et al.[55] from analysis of average total cross sections measured at the Japan Atomic Energy Research Institute (JAERI); Tsubone and colleagues pointed out that the value of S_1 obtained from a statistical analysis of the average cross sections in the unresolved resonance range is strongly correlated to the values of S_0 and to the $l = 0$ effective scattering radius R'; in his final result he fixed S_0 at 1.05×10^{-4}, referring to the value of Olsen and Meszaros,[10] and R' at 9.30 fm. Therefore, due to the strong correlations between the parameters, the comparison between different results is not straightforward. A large S_1 value of 2.42×10^{-4} was obtained by Corvi, Rohr, and Weigmann[32] in the neutron energy range 63.5 to 1548.0 eV from a sample of 57 measured $g\Gamma^l_n$, fitted by a Porter-Thomas distribution normalized to about 100 resonances to take into account the missing small values of $g\Gamma^l_n$. These researchers obtained an average value of 2.52 ± 1.10 meV for $g\Gamma^l_n$ from the corrected sample. It is obvious that the sample of 100 resonances was too small compared to the number of about 200 p-wave resonances that should be found in an energy interval of 1500 eV. Their corrected average value could be overestimated by more than 25%. However, the individual $g\Gamma^l_n$ values of Corvi, which

are given with errors generally larger than 10%, are on average only 2.4% larger than the values of the present evaluation, which is quite good agreement.
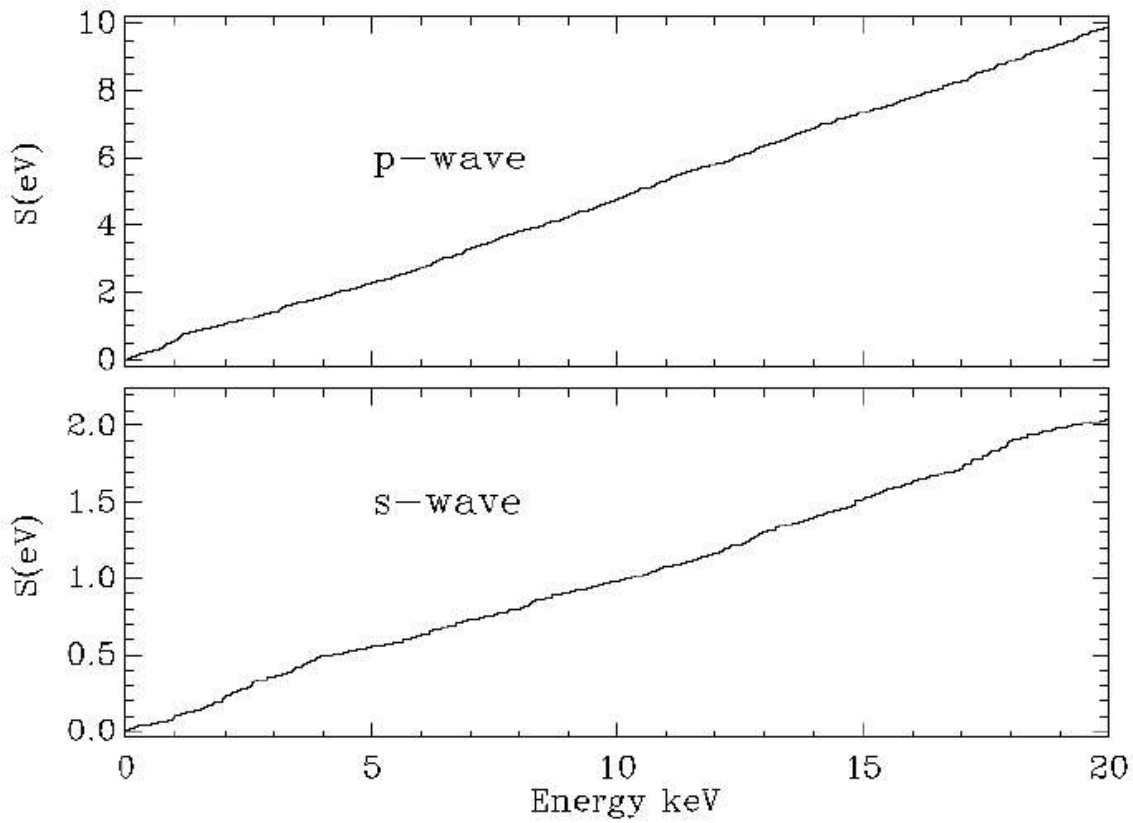
Fig. 26. Variation of the cumulative sum of the reduced neutron widths versus neutron energy for the *s*-wave resonances (lower curve) and the *p*-wave resonances (upper curve).

In the low-energy range, the neutron width values of Olsen were obtained from a multilevel Breit-Wigner least-squares analysis, by the computer code SIOB,[56] of the same experimental transmission data. These values should agree with the present evaluation, since the multilevel Breit-Wigner formalism is almost equivalent to the Reich-Moore formalism for nonfissile nuclei. The s-wave strength function obtained by Olsen in the energy range below 1060 eV was $(0.968 \pm 0.006) \times 10^{-4}$ which compares to the value of $(0.975 \pm 0.006) \times 10^{-4}$ obtained in the present work in the same energy range, the errors being the statistical errors. The difference of 0.7% is mainly due to the parameters in the energy range above 700 eV, where differences of 5 to 20% are observed in neutron widths of several resonances. In the energy range 0.89 to 10 keV, the transmissions taken at the 150-m flight path were fitted by Olsen with all the resonances taken as $J = 1/2$ levels; his sample contains only 676 resonances, which are the resonances observable in the transmission data, against 1457 used in the present work in the same energy range. The important difference between these numbers of resonances is due to the extra resonances seen in the Harvey high-resolution transmission and in the Macklin capture data, and to the small resonances added in the present evaluation to conform with the Porter-Thomas and Wigner distributions. Olsen calculated an s-wave strength function value of 0.940×10^{-4} from his sample of resonances in the energy range 0 to 10 keV, by correcting for the contribution of the p-wave with a p-wave strength function of 1.9×10^{-4}. This value compares with the value of 0.979×10^{-4} obtained in the present work for the same energy range. The difference of 4% could be due to the following: First, the correction for the p-wave contribution should be smaller. Second, the Olsen neutron widths of the large resonances, which agree well, on average, with the present work in the energy range below 6 keV, are systematically smaller by about 2.5% above 6 keV. Third, the larger value of R′ used by Olsen tends to offset the contribution of his missing resonances.

The variation versus energy of the local neutron strength functions, calculated over 1-keV energy intervals, is shown in Fig. 27. The s-wave values are given in the lower part of the figure and the p-wave values in the upper part. The solid squares represent the s-wave values of Olsen in the energy range 0 to 10 keV, showing good agreement with the present results below 6 keV; above 6 keV the Olsen values are 10–20% smaller. Note that taking the present local p-wave strength functions for the correction of the Olsen s-wave values, instead of taking a constant value of 1.9×10^{-4}, would decrease the discrepancy by a significant amount. Doing this between 8 keV and 9 keV, where the value of the p-wave strength function shows a minimum, would decrease the discrepancy from 18% to 9%.

Compared to the previous analyses, significant improvement has been achieved in the present work concerning the accuracy of the neutron widths in the energy range above 6 keV.
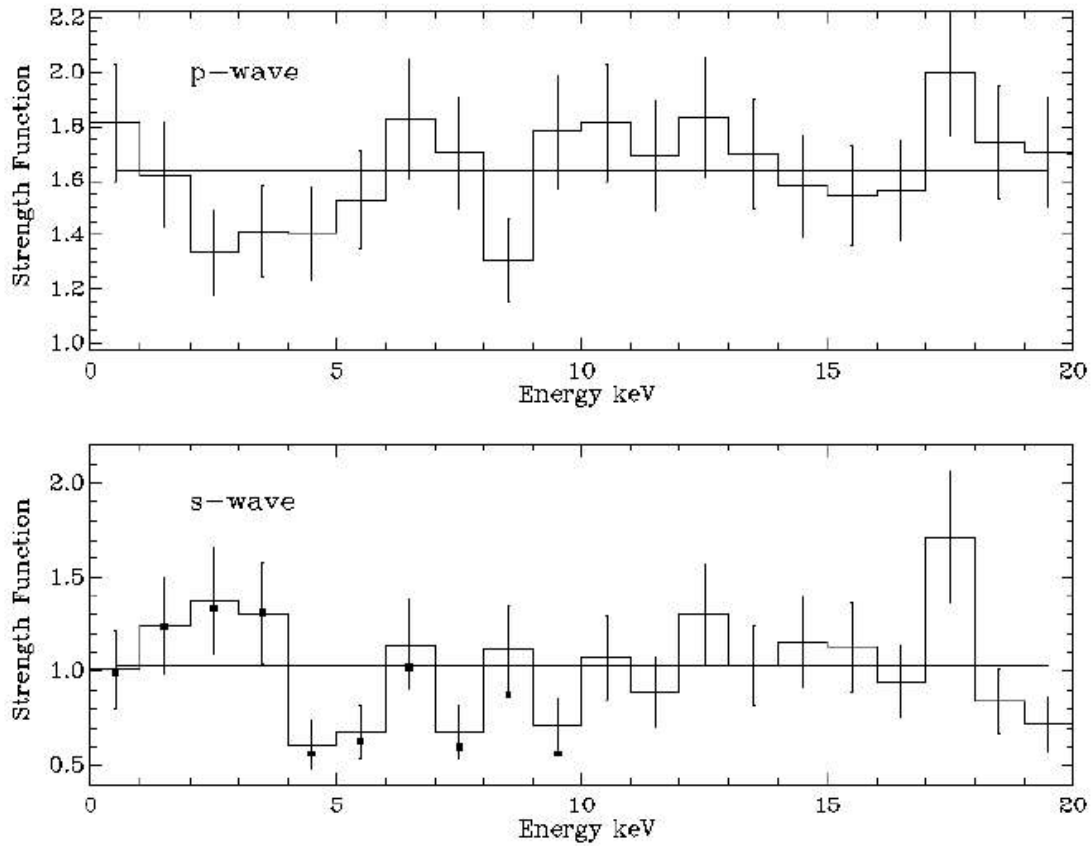
Fig. 27. Histogram of the local values of the neutron strength function in the neutron energy range 0 to 20 keV obtained from the evaluated resonance parameters. The upper part of the figure shows the *p*-wave strength functions. The lower part shows the *s*-wave strength functions. The dark squares are the values obtained by Olsen *et al.* in the energy range 0 to 10 keV.

51

5.5. FISSION WIDTHS

In the energy range 0 to 10 keV, the ENDF/B-VI fission widths in the fission clusters were those obtained by Difilippo *et al.*,[15] or by Sowerby and Moxon from the Difilippo fission area, and were not modified in the present evaluation. In the energy range 10 to 20 keV, five unresolved clusters are seen in the Difilippo fission data. Each cluster is formed by several unresolved class-I resonances. In the present work, the fission widths were distributed between the resonances of the clusters to reproduce the fission area of the clusters. The average fission cross section calculated by SAMMY from the resonance parameters in the energy range 10 to 20 keV is 0.10 mb, in agreement with the Difilippo *et al.* measurements.

5.6. RADIATIVE CAPTURE WIDTH IN THE HIGH-ENERGY RANGE

For all the resonances for which the radiative capture width was not fitted, the value of 23.0 meV (recommended in the Sowerby-Moxon evaluation) was used in the present work. In the energy range 1 to 10 keV, the value of 23.0 meV allows a good fit of the experimental transmission and capture data for about 99% of the resonances. A few resonances have Γ_γ values that could be very different from the average value; these were used to improve the fit of the experimental data and have no physical meaning. In the energy range 10 to 20 keV, about 15% of the resonances have capture widths different from 23.0 meV, some of them being two or three times smaller or larger. Again, these allow a good description of the experimental capture cross section in the corresponding energy regions; however, this description is not unique, and the resonances should be considered to be pseudo-resonances.

Another problem is the effect of the fission clusters on the measured capture cross section. The detector used in the capture measurements did not discriminate between fission and capture gamma rays; a non-negligible part of the capture area could be due to the fission process, for those resonances with relatively large fission areas. This effect has been investigated by Auchampaugh *et al.*[57] in the resonances of the fission clusters near 721 and 1211 eV neutron energy. In the fission clusters, the capture and fission area of the resonances should by calculated with the relations $a_\gamma = \Gamma_n(\Gamma_\gamma + \epsilon\Gamma_f)/\Gamma$ and $a_f = \Gamma_n\Gamma_f/\Gamma$, in which Γ is the total width of the resonance and ϵ is the contribution to the capture area from the fission process. Auchampaugh obtained a_γ from the Macklin capture data, a_f from the Difilippo fission data, and the neutron widths from the Olsen transmission data. The exact value of ϵ, which is a characteristic of the gamma-ray detector used by Macklin, is not known and could depend on the resonances. For $\epsilon = 0$ and 2, the capture widths calculated by Auchampaugh *et al.* for the 721.7 eV resonance were, respectively, 6.6 meV and 3.5 meV. They concluded that the resonance at 721.7 eV was a class-II resonance, the small value of Γ_γ being consistent with a radiative capture width of a state (class II state) in the second well of the double humped fission barrier. The same conclusion was obtained for the resonance at 1211.3 eV, which should have a capture width of 6.6 meV. In the present SAMMY analysis of the experimental data, the effect of the fission on the experimental capture data was not taken into account. This effect could be important in the fission clusters where at least one resonance has a fission area close to 0.2 b eV, which in particular occurs at 721.7 and 1211.3 eV. There are 15

fission clusters in the energy range 2 to 20 keV; some of the *s*-wave resonances of these clusters could have different capture widths from 23 meV. In the present work the Auchampaugh Γ_γ values were assigned to the resonances at 721.7 eV and 1211.3 eV. Other possible modifications were not investigated, but their effect on the calculated average capture cross section should be negligible, since the modifications would concern fewer than 1% of the total number of *s*-wave resonances.

5.7. COVARIANCE MATRICES OF THE RESONANCE PARAMETERS

Due to the size of the experimental database and the number of resonances involved in the SAMMY analysis, a full correlation matrix of the resonance parameters could not be obtained without unrealistic computer space and time. The full ^{238}U resonance parameter correlation matrix will contain more than 6×10^6 different elements if all the parameters are considered. Partial correlation matrices were obtained corresponding to the energy ranges 0.5 to 60 eV, 60 to 250 eV, 250 to 500 eV, 500 to 750 eV, and 750 to 1000 eV, and to interval of 1 keV in the energy range 1 to 20 keV, in which the sequential SAMMY analyses of the experimental data were performed. These correlation matrices show that more than 80% of the correlation coefficients are smaller than 1% in absolute value, and the energy range of the non-negligible correlations between resonance parameters is smaller than 50 eV neutron energy. In general, if one obtains χ^2 values close to 1, the errors on the final parameters are unrealistically small compared with the errors expected from the systematic errors on the experimental data. In SAMMY, fits of consistent data generate small resonance parameter errors; consistency between the experimental data is obtained by using correction parameters for each experimental data set; and the correction parameters are related to the systematic errors on the experimental data. For the current SAMMY evaluation, the correction parameters were included in the calculation of the theoretical function and treated as parameters to be fitted. Measured experimental uncertainties were used for the prior (initial) uncertainty on the correction parameters, so that the effect of these uncertainties was therefore included in the final covariance matrix for the resonance parameters. As examples, in the energy range below 500 eV, SAMMY calculates errors of 0.5 to 1.0% on the neutron widths of the large *s*-wave resonances; in the high energy range above 19 keV the errors calculated for the neutron widths of the large resonances are 3 to 8%, and more than 10% for the small resonances. The resonance parameters and the errors are given in Tables 10–12 in three selected energy ranges.

A method for building a realistic full-parameter covariance file suitable for ENDF/B-VII is under consideration.[58] It consists of identifying the parameters that are important for the calculation of the covariance matrix of group cross sections in order to reduce the size of the parameter correlation matrix and of using more efficient computer environments to allow the analysis of a large experimental database. Note that an option of SAMMY allows the direct calculation of the covariance matrix for group cross sections from the SAMMY covariance file.[59] A partial parameter covariance matrix in the low-energy region could be sufficient for some thermal reactor applications or criticality safety calculations. For these purposes, a ^{238}U covariance file for the parameters of the energy range 0 to 1000 eV has been generated.

Table 10. Resonance parameters in the energy range 0.25 to 0.45 keV

J	*l*	E (eV)	Error	Γγ (meV)	Error	Γn (meV)	Error
1.5	1	253.8984		23.00		0.0487	
0.5	1	257.2334		23.00		0.0237	
1.5	1	263.9772	0.0039	23.00		0.1406	0.0025
0.5	0	273.6901	0.0016	22.65	0.40	25.1324	0.1224
1.5	1	275.2725	0.0102	23.00		0.0953	0.0038
1.5	1	278.2439		23.00		0.0036	
1.5	1	282.4634		23.00		0.0523	
0.5	1	285.7126		23.00		0.0099	
0.5	0	291.0325	0.0018	22.08	0.57	16.6078	
1.5	1	294.2314		23.00		0.0069	
0.5	1	307.9811		23.00		0.0152	
0.5	0	311.3198	0.0014	23.00		0.9432	0.0172
1.5	1	322.6491		23.00		0.0154	
1.5	1	332.0868		23.00		0.0236	
1.5	1	337.2875		23.00		0.0506	
0.5	0	347.8474	0.0019	21.90	0.31	79.9281	0.2496
1.5	1	351.9554		23.00		0.1085	
0.5	0	353.6449		23.00		0.0220	
1.5	1	368.4164		23.00		0.0085	
0.5	1	372.9918		23.00		0.0360	
1.5	1	375.7304		23.00		0.0114	
0.5	0	376.9025	0.0024	23.00		1.3663	0.0193
1.5	1	390.3643		23.00		0.0096	
1.5	1	394.9220		23.00		0.0296	
0.5	0	397.7159	0.0034	13.67	0.95	5.8946	0.0799
1.5	1	407.7953		23.00		0.0330	
0.5	0	410.3021	0.0028	23.10	0.77	19.9367	0.1584
1.5	1	416.2354		23.00		0.0076	
0.5	0	434.0647	0.0019	28.72	1.38	10.1779	0.1223
1.5	1	439.7528		23.00		0.1360	
1.5	1	444.4321		23.00		0.0114	
1.5	1	447.8579		23.00		0.0196	

Table 11. Resonance parameters in the energy range 4.00 to 4.15 keV

J	l	E (eV)	Error	$\Gamma\gamma$ (meV)	Error	Γ_n (meV)	Error
0.5	1	4007.7090		23.00		0.567	0.055
1.5	1	4009.7593	0.0234	23.07	2.29	1.828	0.058
0.5	1	4015.0806	0.0298	23.49	2.31	1.692	0.109
0.5	0	4016.1965	0.0209	22.85	2.28	2.092	0.119
0.5	1	4025.7017	0.0229	22.52	2.27	1.955	0.107
0.5	1	4026.6475		23.00		0.690	0.065
0.5	0	4037.9553		23.00		0.614	0.064
0.5	1	4038.3999	0.0109	24.09	1.16	15.716	0.376
0.5	0	4042.3103	0.0097	26.84	0.49	78.815	0.970
1.5	1	4053.0986		23.00		0.401	0.038
1.5	1	4053.2654		23.00		0.368	0.029
0.5	1	4063.8501		23.00		0.404	0.038
0.5	0	4065.1006	0.0136	22.28	0.6	32.393	0.606
0.5	1	4073.9370		23.00		0.142	0.014
0.5	1	4082.1265	0.0230	18.35	1.76	6.295	0.222
1.5	1	4088.7075		23.00		0.400	0.035
0.5	0	4091.1218	0.0087	28.89	0.48	125.653	1.165
1.5	1	4099.0068		23.00		0.069	0.006
1.5	1	4102.5049	0.0169	23.17	2.30	1.215	0.054
0.5	1	4103.8626		23.00		0.448	0.046
1.5	1	4106.0000		23.00		0.692	0.040
0.5	1	4123.2559	0.0023	22.52	2.18	4.791	0.189
0.5	1	4123.4619		23.00		0.584	0.056
0.5	0	4126.2803	0.0119	27.27	0.67	43.778	0.709
1.5	1	4132.6870	0.0038	23.69	2.28	3.435	0.138
0.5	0	4133.3462	0.0037	21.86	2.20	3.370	0.232
1.5	1	4142.1245		23.00		0.010	0.001
1.5	1	4146.9380		23.00		0.154	0.015
0.5	1	4149.4028	0.0230	22.85	2.22	4.226	0.144

Table 12. Resonance parameters in the energy range 19.00 to 19.15 keV

J	l	E (eV)	Error	Γγ (meV)	Error	Γn (meV)	Error
0.5	0	19007.8418	0.0130	23.00		6.72	0.65
1.5	1	19004.7324	0.0086	23.00		15.09	1.07
0.5	0	19011.0215	0.0729	23.00		367.60	5.81
1.5	1	19016.5215	0.0018	23.00		4.55	0.39
0.5	1	19027.4238	0.0298	23.00		5.53	0.56
0.5	0	19026.6973	0.0733	26.05	2.28	44.40	3.43
1.5	1	19029.8906	0.0316	23.00		2.94	0.28
1.5	1	19030.6797	0.0389	23.00		18.03	1.37
0.5	1	19049.1504	0.0576	23.00		3.77	0.35
0.5	1	19053.2891	0.0099	23.00		26.83	2.23
0.5	0	19054.0254	0.0100	12.17	1.14	22.41	2.06
1.5	1	19060.8438	0.0456	23.00		1.41	0.15
0.5	1	19068.2871	0.0791	23.00		11.51	1.10
0.5	0	19072.9141	0.0120	23.00		117.18	7.89
0.5	1	19076.4160	0.0345	23.00		37.52	3.40
0.5	0	19077.5508	0.1308	23.00		353.40	10.59
0.5	1	19077.0605	0.1231	23.00		19.49	1.88
1.5	1	19091.9727	0.0022	23.00		7.03	0.50
0.5	0	19100.0898	0.1442	23.00		13.72	1.18
1.5	1	19101.3809	0.0037	23.00		4.25	0.36
1.5	1	19113.0156	0.0608	23.00		1.29	0.13
0.5	1	19118.6133	0.0046	23.00		15.43	1.57
0.5	1	19122.0488	0.0775	23.00		1.47	0.15
0.5	0	19125.4102	0.0919	27.96	1.75	275.47	9.32
1.5	1	19127.8965	0.0052	23.00		24.89	2.21
0.5	0	19132.3750	0.0456	14.34	1.24	143.72	10.39
0.5	1	19135.3887	0.0172	18.00		188.71	10.17
1.5	1	19144.1973	0.1065	34.40	1.60	52.53	1.73

6. IMPACT OF THE NEW EVALUATION ON INTEGRAL EXPERIMENT

The ^{238}U resonance parameters comprise one of the most sensitive pieces of nuclear data in the neutronic calculations of thermal critical assemblies. Reactor physicists require the ^{238}U capture cross section to be known with an accuracy better than 1% below 100 eV. To relate the actual ^{238}U reaction rate in reactors to the ^{238}U resonance parameters, the integral parameter known as the effective or shielded resonance integral (SRI) is often used. In classic resonance absorption theory, the neutron flux $\varphi(u)$ is the product of the asymptotic flux (outside the resonances, which is a smooth function of lethargy) and the fine structure function representing the dips of the flux in the vicinity of the resonances. The effective capture resonance integral I_{eff} is then defined as

$$I_{eff} = \int \sigma_\gamma(E) \, \varphi(E) dE/E = \int \sigma_\gamma(u) \, \varphi(u) du \,,$$

in which the lethargy variable u is equal to $\ln(E_0/E)$. The low- and high-energy limits E_{min} and E_{max} of the resonance integral are generally chosen to span the resolved and unresolved resonance range.

In the case of ^{238}U, the self-shielding process is crucial in reactor calculations and can be defined as a function of the dilution or background cross section d. The effective resonance capture integral is much smaller than the usual infinitely dilute resonance integral (i.e., without self-shielding). For instance, the infinitely dilute resonance integral in the present evaluation is 275 barns, while the shielded one, at a dilution representative of light water reactors ($d = 50$ b), is about 55 barns, with $E_{min} = 1$ eV and $E_{max} = 10$ keV. The sensitivity coefficient of the dilute and effective resonance integral with respect to the resonance parameters is also different; while the dilute resonance integral does not depend much on the radiation width of the 6.68-eV resonance, the shielded resonance integral (SRI) will be very sensitive to it. In the present work, the SRI has been checked using the GROUPR module of NJOY,[60] which solves the integral slowing-down equation (actually the fine-structure equation) in homogeneous material assuming isotropic scattering in the center-of-mass system. Compared to the ENDF/B-VI evaluation, the SRI using the present resonance parameters is found to be slightly lower, by 1.0% for infinite dilution and by 0.6% at a dilution of 50 b. The main reason for this reduction is smaller neutron widths below 100 eV. As previously mentioned, the thermal capture value 2.683 b is also reduced compared with the 2.719-b value of ENDF/B-VI. Therefore, the present resonance parameters, giving a slight reduction of the capture cross section in the thermal and epithermal range, will have an impact on the k_{eff} of the thermal lattice and on the other integral parameters such as the usual spectral indices, the conversion ratio, and the production of ^{239}Pu in pressurized water reactors (PWRs).

Trends derived from validation of the most recent major nuclear data libraries, such as ENDF/B-VI.8, JEFF3.0, and JENDL3.3, have pointed out a significant underestimation of the k_{eff} of low-enriched uranium thermal lattices. The present evaluation contributes to improving the k_{eff} prediction. The impact of the new resonance parameters was assessed with the Monte Carlo code MCNP,[61] using several benchmarks from the International Criticality and Safety Benchmark

Evaluation Project (ICSBEP).[62] For illustration purposes, the TCA light-water- moderated critical experiments performed at JAERI[63] and called LEU-COMP-THERM-006 were investigated with the latest ENDF/B-VI evaluation and with the present resonance parameters. The JAERI experiments consist of small critical thermal assemblies using low-enriched UO_2 rods (2.6% of ^{235}U). The level of water in the tank containing the fuel rod lattice was raised until criticality was achieved, and the critical water height was then accurately measured. The uncertainty of the measured k_{eff}, typically about 300 pcm, was mainly due to uncertainties in the measured water height and in the geometry (rod and clad radius, for instance). Various configurations have been measured with water-to-fuel volume ratios ranging from 1.5 to 3.0.

As shown in Table 13, the impact of the present evaluation is an increase by 100 to 150 pcm of the reactivity. Similar improvements in reactivity prediction have been observed for many LEU-COMP- THERM benchmarks in the ICSBEP. While the k_{eff} is still underestimated, it can be shown that an improved evaluation of the inelastic scattering leads to a satisfactory correction of the reactivity bias. More details on this problem can be found in the final report of the NEA/WPEC working group (subgroup-22), to be published.[64]

Table 13. Results of k_{eff} benchmark calculations

ICSBEP database	Water-to-fuel vol. ratio	k_{eff} Values		
		ENDF/B-VI.8	LANL[a]	LANL + ORNL[b]
LCT6-1	1.50	0.99240	0.99634	0.99790
LCT6-4	1.83	0.99299	0.99593	0.99797
LCT6-9	2.48	0.99500	0.99747	0.99818
LCT6-14	3.00	0.99521	0.99778	0.99962

[a] Values of k_{eff} obtained by replacing ^{238}U high energy range of ENDF/B-VI with new LANL evaluation.
[b] Values of k_{eff} obtained by replacing ENDF/B-VI ^{238}U evaluation with a new file obtained by merging new LANL high-energy range with present resonance parameter evaluation.

The postirradiation examination (PIE) provides meaningful information on ^{238}U cross sections. These experiments involve measuring the concentrations of nuclides as a function of burn-up. Using PIE performed on fuel irradiated in a French PWR, it was shown[65] that the ^{239}Pu isotopic ratio (number of atoms of ^{239}Pu over the number of atoms of ^{238}U) is systematically overestimated by 1 to 3% in uranium-oxide and mixed-oxide fuel using the most recent nuclear data library. The slight reduction of the SRI brought by the present evaluation should partially correct this discrepancy; consequently, the prediction of k_{eff} in burn-up calculations should be improved as well. Additionally, the interpretation of spectral indices measured in the EOLE facility in Cadarache, France (the MISTRAL and ERASME experimental program)[65] pointed out a slight overestimation of the ^{238}U reaction rate by 1–2% compared with the previous evaluation, Again, better agreement should be obtained with the present evaluation.

7. CONCLUSIONS

A new evaluation of the [238]U resonance parameters was obtained from a SAMMY Bayesian analysis of the most recent high-resolution neutron transmission and capture cross section measurements. This evaluation complements the Sowerby-Moxon[1] evaluation used in the most important evaluated data libraries in the energy range 0 eV to 10 keV, by completing the analysis of the Macklin *et al.* capture measurements and by adding to the experimental database the Harvey *et al.* high-resolution transmission data. This evaluation also extends the resolved resonance range from the previous 10 keV to 20 keV.

The new evaluation was tested by several benchmark calculations; significant improvements were obtained in reactivity predictions. The extension of the resolved resonance range to the neutron energy of 20 keV will allow more accuracy in the calculation of self-shielding factors. Study of the statistical properties of the resonance parameters allowed an accurate determination of the average value of the parameters for more reliable model calculations of the cross sections in the high-neutron-energy range. The recommended value of the average resonance parameters are given in Table 14. For the first time, a recommendation can be given for an average *p*-wave capture width, on the basis of the analysis of four *p*-wave resonances in the energy range up to 500 eV; the recommended value is 21.1 ± 2.0 meV, which is smaller than the value of 23.2 ± 1.0 meV obtained from 31 *s*-wave resonances in the energy range up to 1 keV. However, due to the large uncertainty in the *p*-wave resonance value, the two values are not inconsistent.

Table 14. Recommended values for average resonance parameters

	Resonance spacing (eV)	Neutron strength function	Capture width (meV)
s-wave	21.19 ± 0.55	$(1.025 \pm 0.047) \times 10^{-4}$	23.1 ± 1.0
p-wave	7.06 ± 0.20	$(1.70 \pm 0.20) \times 10^{-4}$	21.1 ± 2.0

The results of the present evaluation, which, for the lower-energy part of the data, was a collaboration between ORNL and the Centre d'Etudes de Cadarache (Commissariat à l'Energie Atomique, France), is proposed for the ENDF/B-VII library and for the European JEFF-3 library. However, due to complementary analyses performed after the release of the resonance parameter file, some parameters or average values appearing in the present report could be slightly different from those which could be calculated from the released file.

8. REFERENCES

1. M. G. Sowerby and M. Moxon, "Summary of the Work of the NEANDC Task Force on U-238," NEANDC-313U, Nuclear Energy Agency OECD, Paris, France (1994).

2. A. Courcelle, "Needs for Nuclear Data Measurements to Improve LEU-LWR Reactivity Prediction," Note to WPEC Sub-group 22 (2003).

3. J. A. Harvey *et al.*, "High Resolution Transmission Measurements on ^{235}U, ^{239}Pu, and ^{238}U," *Nuclear Data for Science and Technology*, May 30–June 3, 1988, Mito, Japan (1988).

4. R. L. Macklin *et al.*, "High Resolution Measurement of the ^{238}U Neutron Capture Yield from 1 to 100 keV," *Ann. Nucl. Energy*, **18(10)**, 567 (1991).

5. N. M. Larson, *Updated Users' Guide for SAMMY*, ORNL-9179/R6 (ENDF-364), UT-Battelle, LLC, Oak Ridge National Laboratory, 2003.

6. A. Meister *et al.*, "Experimental Study of the Doppler Broadening of Neutron Resonances at GELINA," pp. 435–439 in *Conference on Nuclear Data for Science and Technology*, Trieste, (Italy), May 19–24, 1997 (1998).

7. D. K. Olsen *et al.*, "Precise Measurement and Analysis of Neutron Transmission through Uranium-238," *Nucl. Sci. Eng.* **62(3)**, 479 (1977).

8. D. K. Olsen *et al.*, "Measurement and Resonance Analysis of Neutron Transmission through Uranium-238," *Nucl. Sci. Eng.* **69(2)**, 202 (1979).

9. D. K. Olsen *et al.*, "Note on ^{238}U+ n Resolved Resonance Energies," *Nucl. Sci. Eng.* **66(1)**, 141 (1978).

10. D. K. Olsen and P. S. Meszaros, "Resolved Resonance Parameters for U from 4 to 6 keV," *Nucl. Sci. Eng.* **83(1)**, 174 (1983).

11. D. K. Olsen, "Resolved Resonance Parameters for ^{238}U from 1 to 10 keV," *Nucl. Sci. Eng.* **94(1)**, 102 (1986).

12. G. de Saussure *et al.*, "Measurement of the ^{238}U Capture Cross Section for Incident Neutron Energy up to 100 keV," ORNL/TM-4059, Union Carbide Corporation (Nuclear Division), Oak Ridge National Laboratory, 1973.

13. W. P. Poenitz, L. R. Fawcett, Jr., and D. L. Smith, "Measurement of the ^{238}U(n,γ) Cross Sections at Thermal and Fast Neutron Energies," *Nucl. Sci. Eng.* **78(3)**, 239 (1981).

14. F. Corvi and G. Fioni, "Shape of the [238]U Neutron Capture Cross Section in the Range 0.002–0.1 eV," paper presented at International Conference on Nuclear Data for Science and Technology, Mito, Japan, 1988.

15. F. C. Difilippo, "[238]U Neutron-Induced Fission Cross Section for Incident Neutron Energies between 5 eV and 3.5 MeV," *Phys. Rev. C* **21(4)**, 1400 (1980).

16. S. F. Mughabghab, *Neutron Cross Section,* vol. 1, part B, pp. 92–30, Academic Press, New York, 1984.

17. J. D. James, "Neutron Energy Standards, *Proc. Int. Specialists Symp. Neutron Standard and Application,* National Bureau of Standards, Gaithersburg, Maryland, 1977.

18. C. W. Reich and M. S. Moore, "Multilevel Formula for the Fission Process," *Phys. Rev.* **111(3)**, 929–933 (1958).

19. J. A. Harvey, private communication, Oak Ridge National Laboratory, 2002.

20. H. Derrien, G. de Saussure, and R. B. Perez, "R Matrix Analysis of [239]Pu Neutron Cross Sections in the Energy Range up to 100 eV," *Nucl. Sci. Eng.* **106**, No. 4, 434 (1990).

21. W. E. Lamb, "Capture of Neutrons by Atoms in a Crystal," *Phy. Rev.* **52**, 295 (1937).

22. D. Naberejnev, C. Mounier, and R. Sanchez, "The influence of Crystalline Binding on Resonant Absorption," *Nucl. Sci. Eng.* **131**, 222–229 (1999).

23. M. G. Sowerby, G. H. Patrick, and D. S. Mather, "The Simultaneous Evaluation of the Fission Cross Sections of [235]U, [239]Pu and [238]U and the Capture Cross Sections of [238]U in the Energy Range 100 eV to 29 MeV, AERE-M2497, EANDC(UK)138AL, Harwell, U.K., 1972.

24. A. M. Lane and J. E. Lynn, "Anomalous Radiative Capture in the Neutron Resonance Region: Analysis of the Experimental Data on Electric Dipole Transitions," *Nucl. Phys.* **17(563)**, 586–608 (1960).

25. G. Arbanas, ORNL, private communication, 2005.

26. F. H. Froehner, "Evaluation of the Unresolved Resonance Range of [238]U," *Nucl. Sci. Eng.* **103**, 119–128 (1988).

27. L. E. Kasakov, *Yad. Const.*, **3**, 37 (1986).

28. N. M. Larson and K. N. Volev, "Validation of Multiple Scattering Corrections in the Analysis Code SAMMY," paper presented at *PHYSOR 2002*, Seoul, Korea, October 7–10, 2002.

29. G. Noguere, "Measurements and Analysis of the I-127 and I-129 Neutron Capture Cross Sections," Ph.D. thesis, 2005.

30. A. Courcelle and H. Derrien, "Statistical Analysis of 238U Cross Section in the Unresolved Energy Range," to be prepared for *Nucl. Sci. Eng*. (2006).

31. M. C. Moxon, *The Neutron Capture Cross Section of ^{238}U in the Energy Region 0.5 to 100 keV*, AERE-R-6074, Atomic Energy Authority, Harwell, U.K., 1969.

32. F. Corvi, G. Rohr, and H. Weigmann, "p-Wave Assignment of ^{238}U Neutron Resonances," p. 733 in *Proc. Conf. Neutron Cross Sections and Technology,* NBS-425, National Bureau of Standards Washington, D.C., 1975.

33. F. Gunsing *et al.*, "Spins of Resonances in Reactions of Neutrons with ^{238}U and ^{113}Cd, *Phys. Rev. C* **56(3)**, 1266 (1997).

34. B. E. Crawford *et al.*, "Parity Nonconservation in Neutron Resonances in ^{238}U," *Phys. Rev. C* **58(2)**, 1225 (1998).

35. C. E. Porter and R. G. Thomas, "Fluctuations of Nuclear Reaction Widths," *Phys. Rev.* **104(2)**, 483–491 (1956).

36. E. P. Wigner, "Results and Theory of Resonance Absorption," in *Proc. of Conference on Neutron Physics by Time of Flight*, Gatlinburg, TN, 1956; ORNL-2309, Union Carbide Corporation (Nuclear Division), Oak Ridge National Laboratory, 1957.

37. F. W. K. Firk, J. E. Lynn, and M. C. Moxon, "Resonance Parameters of the Neutron Cross Section of U^{238}," *Nucl. Phys*. **41**, 614–629 (1963).

38. J. B. Garg *et al.*, "Neutron Resonance Spectroscopy. III. Th^{232} and U^{238}," *Phys. Rev.*, **134(5B)**, B985–B1009 (1964).

39. L. M. Bollinger *et al.*, " Neutron Resonance Structure of Uranium-238," *Phys. Rev.* **105(2)**, 661–665 (1957).

40. G. Carraro and W. Kolar, in *Proc. Int. Conf. Nuclear Data for Reactors*, Helsinki IAEA-CN-26/116, 1, 403, IAEA, Vienna, 1970.

41. K. H. Maletski, *et al.*, *Sov. T. At. Energy* **32**, 45 (1972).

42. F. Rahn *et al.*, " Neutron Resonance Spectroscopy. X. ^{232}Th and ^{238}U," *Phys. Rev. C*, **6**, 1854–1869 (1972).

43. Y. Nakajima *et al.*, p. 738 in *Proc. Conf. Neutron Cross Sections and Technology*, NBS-425, National Bureau Standards, Washington, D.C., 1975.

44. R. E. Chrien and H. I. Liou, p. 1298 in *Proc. Int. Conf. Interaction of Neutrons with Nuclei,* CONF-760715–P2, University of Lowell, 1976.

45. Seminar on [238]U Resonance Capture, March 18–20, 1975, BNL-NCS-50451 (1975).

46. A. Trkov *et al.*, "Revisiting the [238]U Thermal Capture Cross Section and Gamma Emission Probabilities from [239]Np Decay," paper submitted to *Nucl. Sci. Eng.*, 2004.

47. M. Atoji *et al.*, " Slow-Neutron Scattering Cross Sections of Terbium, Ytterbium, and Lutetium," *Phys. Rev.* **121** (1961).

48. R. B. Roof, G. P. Arnold, and K. A. Gschneider, "Nuclear Coherent Scattering Amplitudes for Thorium, Uranium, and Plutonium," *Acta Cryst*. **15**, 351–352 (1962).

49. B. T. M. Willis, *Proc. Roy. Soc. London,* Ser. A, **274**, 122–133 (1963).

50. L. Koestler, R. Knopf, and W. Waschkowski, "Scattering Lengths and Resonance Parameters," *Proc. Int. Conf. Neutron Physics and Nuclear Data*, Harwell, U.K., Sept. 1988, OECD, 1978.

51. A. Boeuf, *et al.*, "Neutron Interferometric Determination of the Coherent Scattering Length of Natural Uranium," *Phys. Rev. Lett.* **49(15)**, 1086 (1982).

52. A. Courcelle, G. Noguere, and N. M. Larson, "Experimental Tests of the Crystal Lattice Model of SAMMY," *Int. Conf. Nuclear Data for Science and Technology*, Santa Fe, N.M., 2004.

53. A. Courcelle, H. Derrien, and L. C. Leal, "Statistical Study of [238]U Resonance Parameters," to be prepared for *Nucl. Sci. Eng*. (2006).

54. H. Derrien *et al.*, "Average Neutron Cross Sections in the Unresolved Resonance Energy Range from ORELA High Resolution Transmission Measurements," ORNL/TM-2003/291, UT-Battelle, LLC, Oak Ridge National Laboratory, 2003.

55. I. Tsubone *et al.*, "Neutron Total Cross Sections of [181]Ta and [238]U from 24.3 keV to 1 MeV and Average Resonance Parameters," *Nucl. Sci. Eng.* **88(4)**, 579 (1984).

56. G. de Saussure, D. K. Olsen, and R. B. Perez, *SIOB: A Fortran Code for Least-Square Shape-Fitting of Several Neutron Transmission Measurements Using the Breit-Wigner Multilevel Formula*, ORNL/TM-6286, Union Carbide Corporation (Nuclear Division), Oak Ridge National Laboratory, 1978.

57. G. F. Auchampaugh, *et al.*, "Resolution of the Nature of the Coupling in Subthreshold Fission in ^{238}U+ n," *Phys. Rev. C* **33(1)**, 125 (1986).

58. L. C. Leal and G. Arbanas, private communication, Oak Ridge National Laboratory, 2005.

59. H. Derrien, N. M. Larson, and L. C. Leal, *Covariance Matrices for Use in Criticality Safety Predictability Studies*, ORNL/TM-13492, UT-Battelle, LLC, Oak Ridge National Laboratory, 2001.

60. R. E. MacFarlane, *The NJOY Nuclear Data Processing System Version 91*, LA-12740-M, Los Alamos National Laboratory, Los Alamos, N.M., 1994.

61. F. B. Brown *et al.*, *MNCP: A General Monte Carlo N-Particle Transport Code, Version 5*, LA-UR-1987, Los Alamos National Laboratory, Los Alamos, N.M., 2003.

62. *International Handbook of Evaluated Criticality Safety Benchmark Experiments,* NEA/NSC/DOC(95)03, OECD Nuclear Energy Agency, September 2003.

63. Y. Miyoshi and T. Arakawa, *Critical Arrays of Low-Enriched UO$_2$ Fuel Rods with Water-to-Fuel Volume Ratios of 1.5 to 3.0*, NEA/NSC/DOC/(95)03/IV ICSBEP LEU-COMP-THERM-006, vol. IV, Rev. 2, November 15, 1999.

64. A. Courcelle, *Final Report of the WPEC/Subgroup-22: Nuclear Data for Improved Reactivity Prediction*, OECD/NEA/WPEC, to be published.

65. A. Courcelle, *et al.*, "Experimental Validation of Main Fission Products and Actinide Nuclear Data: Improvements for JEFF-3," *Proc. Int. Conf. PHYSOR 2002,* Seoul, Korea, October 7–10, 2002.

INTERNAL DISTRIBUTION

1. G. Arbanas, 5700, MS 6171	13. L. C. Leal, 5700, MS 6171
2. W. C. Carter, 5700, MS 6170	14. J. M. Norman, 4500N, MS 6227
3. K. Clarno, 5700, MS 6172	15. D. K. Olsen, 8600, MS 6442
4. H. Derrien, 5700, MS 6171	16. C. V. Parks, 5700, MS 6170
5. M. E. Dunn, 5700, MS 6170	17. J. E. Rushton, 4500N, MS 6243
6. J. B. Echols, 5700, MS 6171	18. R. O. Sayer, 5700, MS 6171
7. C. W. Forsberg, 5700, MS 6179	19. J. C. Wagner, 5700, MS 6170
8. J. C. Gehin, 5700, MS 6712	20. R. M. Westfall, 5700, MS 6170
9. N. M. Greene, 5700, MS 6171	21. D. Wiarda, 5700, MS 6171
10. K. H. Guber, 5700, MS 6171	22. M. L. Williams, 5700, MS 6170
11. J. O. Johnson, 5700, MS 6172	23. ORNL OTIC–RC, 6011, MS 6283
12. N. M. Larson, 5700, MS 6171	

EXTERNAL DISTRIBUTION

24. F. A. Alpan, Westinghouse Electric Company Nuclear Services, Mail Bin 18, P.O. Box 158, Madison, PA 15663 (alpanfa@westinghouse.com)

25. P. Blaise, DER/SPRC/LEPH, Batiment 230, Centre d'Etudes de CADARACHE, 13108 Saint Paul-lez-Durance, FRANCE

26. Olivier Bouland,CEA/DEN/DER/SPRG/LEPh, Cadarache Centre, F-13108 Saint-Paul-lez-Durance Cedex, FRANCE

27. A. Brusegan, Central Bureau for Nuclear Measurements, Steenweg op Retie, 2240 Geel, BELGIUM

28. J. Burke, Gaerttner LINAC Laboratory Rensselaer Polytechnic Institute, Department of Environmental and Energy Engineering, Troy, NY 12180-3590

29. D. Cabrilla, U.S. Department of Energy, NE-40, 19901 Germantown Road, Germantown, MD 20874-1290

30. Allan D. Carlson, Ionizing Radiation Division, National Institute of Standards and Technology, Gaithersburg, MD 20899

31. D. E. Carlson, U.S. Nuclear Regulatory Commission, Reactor and Plant System Branch, Division of System Research, Office of Nuclear Regulatory Research, MS T-10 G6, Rm. T-10, 17, Washington, DC 20555-0001

32. M. B. Chadwick, Los Alamos National Laboratory, MS B243 T-16, Los Alamos, NM 87545

33. J. Chang, Korea Atomic Energy Research Institute, Nuclear Data Evaluation Laboratory, P.O. Box 105, Yusang, Taejon 305-600, KOREA

34. Arnauld Courcelle, CEA/DEN/DER/SPRG/LEPh, Cadarache Centre, F-13108 Saint-Paul-Lez-Durance Cedex, FRANCE

35. Patrick Cousinou, Institut de Radioprotection et de Surete Nucleaore, B.P. 17, 92262 Fontenay-aux-Roses, FRANCE

36. D. H. Crandall, NA-11/Forrestal Building, U.S. Department of Energy, 1000 Independence Ave., Washington, DC 20585

37. D. E. Cullen, Lawrence Livermore National Laboratory, MS-L-298, P.O. Box 808, Livermore, CA 94550

38. Y. Danon, Gaerttner LINAC Laboratory, Rensselaer Polytechnic Institute, Department of Environmental and Energy Engineering, Troy, NY 12180-3590

39. Jean-Pierre Delaroche, Department de Physique Theorique et Appliquee CEA/DAM, B.P. 12, F91680, Bruyere-Le Chatel, FRANCE

40. Emmeric Dupont, CEA/DEN/DER/SPRG/LEPh, Cadarache Centre, F-13108 Saint-Paul-Lez-Durance Cedex, FRANCE

41. J. R. Felty, Science Applications Intl. Corp., 2418 N. Dickerson St., Arlington, VA 22207

42. P. Finck, Argonne National Laboratory, Reactor Analysis Division, Bldg. 208, Argonne, IL 60439

43. S. C. Frankle, X-TM, MS B226, Los Alamos National Laboratory, Los Alamos, NM 87545

44. W. Furman, Frank Laboratory of Neutron Physics, JINR, Dubna, RUSSIA

45. C. Gould, North Carolina State University, Physics Dept., Box 8202, Raleigh, NC 27695-8202

46. F. Gunsing, Centre D'Etudes De Saclay, F-Saclay - 91191, Gif-sur-Yvette Cedex, FRANCE

47. Robert Haight, Los Alamos National Laboratory, Los Alamos, NM 87545

48. A. Hasegawa, Nuclear Data Center, Japan Atomic Energy Research Institute, Tokai-mura, Naka-gun, Ibaraki-ken 319-11, JAPAN

49. M. Herman, National Nuclear Data Center, Bldg. 197D, Brookhaven National Laboratory, Upton, NY 11973-5000

50. D. Hwaug, Argonne National Laboratory, Reactor Analysis Division, Bldg. 208, Argonne, IL 60439

51. Tatania Ivanova, State Scientific Center of the Russian Federation, Institute for Physics and Power Engineering, Bondarenko Sq, Obninsk, Kaluga Region, 249020, RUSSIAN FEDERATION

52. M. Jaeger, Inst. F. Strahlenphysik, Allmandring 3, Stuttgart D-70569, GERMANY

53. N. Janeva, Bulgarian Academy of Sciences, 72, Boul, Tzarigradsko shosse, Sofia 1784, BULGARIA

54. H. C. Johnson, U.S. Department of Energy, EM-21 Forrestal, 1000 Independence Ave., SW., Washington, DC 20585

55. Toshihiko Kawano, Los Alamos National Laboratory, MS B243, T-16, Los Alamos, NM 87545

56. Lambros Lois, U.S. Nuclear Regulatory Commission, 08 E23, 11555 Rockville Pike, Rockville, MD 20852-2746

57. G. Leinweber, Gaerttner LINAC Laboratory, Rensselaer Polytechnic Institute, Dept. of Environmental and Energy Engineering, Troy, NY 12180-3590

58. R. Little, Los Alamos National Laboratory, X-TM, MS B226, Los Alamos, NM 87545

59. M. Lubert, Gaerttner LINAC Laboratory, Rensselaer Polytechnic Institute, Dept. of Environmental and Energy Engineering, Troy, NY 12180-3590

60. C. Lubitz, Knolls Atomic Power Laboratory, P.O. Box 1072, Schenectady, NY 12301

61. R. E. MacFarlane, Los Alamos National Laboratory, T-2, MS B243, Los Alamos, NM 87545

62. Robert McBroom, U.S. Department of Energy, Oak Ridge Operations Office, 200 Administration Road, Oak Ridge, TN 37831

63. Jerry McKamy, EH-21 Germantown Building 270CC, U.S. Department of Energy, 1000 Independence Ave., SW, Washington, DC 20585-1290

64. Richard D. McKnight, Nuclear Engineering Division – Bldg. 208, Argonne National Laboratory, 9700 S. Cass Ave., Argonne, IL 60439

65. Russell D. Mosteller, Applied Physics Division, Los Alamos National Laboratory, Los Alamos, NM 87545

66. C. Mounier, CEN Saclay, DMT/SERMA/LENR, 91191 Gif Sur Yvette Cedex, FRANCE

67. M. C. Moxon, 3 Hyde Copse, Marcham, Abingdon, Oxfordshire, ENGLAND

68. S. F. Mughabghab, Brookhaven National Laboratory, Advanced Technology
    Building 197d, Upton, NY 11973-5000

69. Mark Nikolaev, State Scientific Center of the Russian Federation, Institute for Physics and
    Power Engineering, Bondarenko Sq, Obninsk, Kaluga Region, 249020, RUSSIAN
    FEDERATION

70. C. Nordborg, OECD/NEA, Le Seine St-Germain 12, Boulevard des Iles, 92130,
    Issy-les-Moulineaux, FRANCE

71. P. Oblozinsky, National Nuclear Data Center, Bldg. 197D Brookhaven National
    Laboratory, Upton, NY 11973-5000

72. S. Y. Oh, Nuclear Data Evaluation Lab. Korea Atomic Energy Research Institute,
    P.O. Box 105, Yusung Taejon, 305-600 KOREA

73. A. Plompen, Central Bureau for Nuclear Measurements, Steenweg op Retie, 2240 Geel,
    BELGIUM

74. A. Popov, Frank Laboratory of Neutron Physics, Joint Institute for Nuclear Research,
    RU-141980 Dubna, Moscow Region, RUSSIA

75. C. Raepsaet, CEN Saclay, DMT/SERMA/LEPP, 91191, Gif Sur Yvette Cedex, FRANCE

76. Kevin Reynolds, U.S. Department of Energy, Oak Ridge Operations Office,
    200 Administration Road, Oak Ridge, TN 37831

77. Pascal Romain, Department de Physique Theorique et Appliquee, CEA/DAM, B.P. 12,
    F91680, Bruyere-Le Chatel, FRANCE

78. Veronique Rouyer, Institut de Radioprotection et de Surete Nucleaire, BP 17, 92262
    Fontenay-aux Roses, FRANCE

79. P. Rullhusen, Central Bureau for Nuclear Measurements, Steenweg op Retie, 2240 Geel,
    BELGIUM

80. P. Schillebeeckx, Central Bureau for Nuclear Measurements, Steenweg op Retie,
    2240 Geel, BELGIUM

81. O. A. Shcherbakov, Petersburg Nuclear Physics Institute, 18 8 350 Gatchina, Leningrad
    District, RUSSIA

82. R. Shelley, Central Bureau for Nuclear Measurements, Steenweg op Retie, 2240 Geel,
    BELGIUM

83. K. Shibata, Nuclar Data Center, Japan Atomic Energy Research Institute, Tokai-mura
    Naka-gun, Ibaraki-ken 319-11, JAPAN

84. R. Slovacek, Gaerttner LINAC Laboratory, Rensselaer Polytechnic Institute, Dept. of Environmental and Energy Engineering, Troy, NY 12180-3590

85. H. Takano, Nuclear Data Center, Japan Atomic Energy Research Institute, Tokai-mura, Naka-gun, Ibaraki-ken 319-11, JAPAN

86. M. A. Thompson, NA-117/Germantown Building GTN, U.S. Department of Energy, 1000 Independence Ave., SW, Washington, DC 20585-1290

87. Anatoly Tsiboulia, State Scientific Center of the Russian Federation, Institute for Physics and Power Engineering, Bondarenko Sq. Obninsk, Kaluga Region, 249020, RUSSIAN FEDERATION

88. C. Wagemans, Central Bureau for Nuclear Measurements, Steenweg op Retie, 2240 Geel, BELGIUM

89. J. J. Wagschal, Racah Institute of Physics, The Hebrew University of Jerusalem, 91904, Jerusalem, ISRAEL

90. K. Yoo, Korea Atomic Energy Research Institute, Nuclear Data Evaluation Laboratory, P.O. Box 105, Yusung, Taejon 305-600, KOREA

91. Phillip G. Young, Los Alamos National Laboratory, MS B243 T-16, Los Alamos, NM 87545